JOURNAL OF GEOPHYSICAL RESEARCH, VOL. 99, NO. C9, PAGES 18,447–18,466, SEPTEMBER 15, 1994

Transient temperature and sea level response of a two-dimensional ocean-climate model to greenhouse gas increases

L. D. Danny Harvey

Department of Geography, University of Toronto, Toronto, Ontario, Canada

Abstract. A two-dimensional dynamical ocean model is coupled to an energy balance climate model and used to investigate the transient surface temperature and sea level response to greenhouse gas increases. For most experiments a step function surface-troposphere heating perturbation of 6 W m^{-2} is applied. A transient reduction in the thermohaline overturning flux of 15-30% occurs in most experiments, although in some cases a near-total circulation collapse occurs within the first 100 years and lasts 700-1000 years. The transient circulation decrease is attributed to the greater rate of downward penetration of the heating anomaly in downwelling rather than in upwelling regions and is not a result of reduced convection. For experiments in which the steady state circulation is qualitatively unchanged after a heating perturbation, the surface temperature response is roughly uniform with latitude, in the absence of ice and snow. However, in some cases a heating perturbation induces the transition from a one-cell to a two-cell overturning circulation, or causes a complete reversal in the direction of overturning when a single cell spans both hemispheres, causing marked latitudinal variations in the surface temperature response. The *e*-folding response time scale τ_e for global mean surface temperature ranges from 10 to 142 years as the vertical diffusion coefficient K_v varies from 1 x 10^{-5} m^2 s^{-1} to 5 x 10^{-4} m^2 s^{-1}, but the variation of τ_e with K_v is not uniform due to changes in the transient circulation response as K_v is varied. The one-dimensional upwelling diffusion and pure diffusion models have a significantly faster surface transient response than the two-dimensional (2-D) model, due to transient weakening of thermohaline overturning in the 2-D model, which dampens surface temperature warming. The presence of convection has a small effect on the transient response. Transient sea level rise is highly sensitive to K_v, with faster sea level rise associated with larger K_v and hence with slower surface warming. The steady state ocean warming is approximately uniform with depth and equal to the global mean surface warming (3°C for 6 W m^{-2} forcing) in most experiments, which produces a sea level rise of 2 to 3 m due to thermal expansion. The times required to reach 50% and 75% of the steady state sea level rise are 200-1100 years and 500-2400 years, respectively. However, if the unperturbed circulation consists of a single overturning cell and a second thermohaline overturning cell develops in response to a heating perturbation, vertical mean steady state deep ocean warming and associated sea level rise can be reduced by almost a factor of 10.

Introduction

Because of their ability to absorb and release large quantities of heat, the oceans exert a significant influence on the transient surface temperature response to surface-troposphere heating resulting from the increase of greenhouse gases. *Harvey and Schneider* [1985], utilizing a one-dimensional, globally averaged upwelling-diffusion model, investigated the effect of changes in the vertical diffusion coefficient and upwelling velocity on the transient temperature response to step function GHG increases and the potential role of feedback processes between surface temperature change, the temperature of bottom water formation, the vertical diffusion coefficient, and the upwelling velocity. Among other results, they found that a reduction in the upwelling velocity as the ocean mixed layer temperature warms delays the mixed layer warming, while an increase in upwelling velocity could cause the surface temperature to initially overshoot its steady state response. *Watts* [1985] showed that an externally imposed variation in upwelling velocity can cause significant surface temperature variations on a decadal to centuries timescale. *Gaffin et al.* [1986] investigated the impact of a nonlinear feedback between upwelling velocity and surface temperature change in a globally averaged upwelling-diffusion model and found that, after a small initial perturbation, the model generated self-sustained oscillations with a period of about 80 years. *Piehler and Bach* [1992] applied this feedback in a coupled, upwelling-diffusion climate-carbon cycle model. The Intergovernmental Panel on Climate Change utilized one-dimensional models in generating scenarios of globally

Paper number 94JC00970.
0148-0227/94/94JC-00970$05.00

averaged surface temperature change associated with alternative GHG emission pathways [Bretherton et al. 1990].

Coupled, three-dimensional atmosphere-ocean general circulation models (A/O GCMs) have also been used to investigate the transient response to GHG increases (recent studies include those of *Schlesinger and Jiang* [1988], *Washington and Meehl* [1989], *Stouffer et al.* [1989], *Manabe et al.* [1991, 1992], and *Manabe and Stouffer,* [1993]. *Stouffer et al.* [1989] have shown that a reduction in the intensity of thermohaline overturning in the North Atlantic Ocean can substantially reduce the high-latitude temperature response during the initial decades of the transient response to a GHG increase and that deep oceanic mixing can substantially delay high-latitude warming in the southern hemisphere.

However, there is a need for further analysis and diagnosis of the role of the ocean in the transient response to GHG increases. In this paper a two-dimensional (latitude-depth) ocean model is coupled to an energy balance climate model and used to investigate the impact on the transient response of changes in, and feedbacks involving, ocean mixing parameters. In particular, this paper investigates the latitude-depth evolution of ocean temperature change over time; the time variation of convective, diffusive, and advective heat fluxes between the mixed layer and deep ocean; and the sensitivity of the transient and steady state response to changes in the vertical diffusion coefficient K_v. The transient response of the two-dimensional model is compared with that of the one-dimensional model, and reasons for differences are elucidated. Unlike the one-dimensional upwelling-diffusion model, in which K_v and upwelling velocity w can be varied independently of one another, a change in K_v in the two-dimensional model induces a change in w which has a competing effect on the transient response.

The model used here has a single, zonally averaged ocean basin. For some parameter values the overturning circulation resembles that of the Atlantic Ocean alone rather than the globally averaged observations. Thus rather than being a reliable indicator of the global net effect on the transient surface temperature response of ocean circulation changes (a goal which will probably elude even A/O GCMs for some time), the present study should be regarded as a diagnosis of the impact of specific ocean circulation changes that could occur in individual ocean basins, either starting from the present climate or under different climatic regimes that might exist in the future or could have existed in the past. Thus the present model is a tool in sharpening our insight concerning potential ocean-climate feedback processes which might be applicable both to prospective future climatic change and to past climatic fluctuations.

In all of the experiments presented here the latitudinal patterns of precipitation and zonal surface winds (which drive shallow overturning cells in the ocean) are fixed. A poleward shift of middle latitude precipitation is likely to occur with global warming, and might be expected to lead to a weakening of the thermohaline circulation. However, weakening of the thermohaline circulation occurs in the present model even without a shift of precipitation, so it is worthwhile, as a first step, to study ocean circulation-climate feedback for the simplified case of a fixed precipitation pattern. Furthermore, sensitivity studies, using the model presented here, indicate that imposing a poleward shift of the mid-latitude precipitation belt as the climate warms in response to an external heating perturbation has negligible effect on the transient or steady state temperature or circulation response.

Model Description

The ocean model, described in detail by *Harvey* [1992], is coupled to the energy balance climate model and sea ice model of *Harvey* [1988a, b]. These models are briefly described below for the readers' convenience.

Surface Climate and Sea Ice Models

The energy balance climate model has surface-air, land-sea, and latitudinal resolution, and is forced with diurnally averaged but seasonally varying insolation. The surface layer in the oceanic part of each zone consists of an isothermal mixed layer which, here, is assumed to be 75 m thick between 66°S to 66°N and 100 m thick poleward of these latitudes. Meridional transport of heat in the atmosphere occurs by diffusion.

The latitudinal and seasonal variation of precipitation is prescribed from observations and scaled so that global precipitation equals global evaporation on each time step. Zonally averaged zonal surface winds are also prescribed from observations and used as an upper boundary condition to the ocean model. Surface-air fluxes of latent and sensible heat are computed from bulk aerodynamic formulae with a stability-dependent drag coefficient.

Vertical growth of sea ice is computed using *Semtner's* [1976] zero-layer model with minor modifications. Growth of new ice in leads results in a gradual increase of ice extent, while both vertical and lateral melting occur and lead to a gradual decrease of ice extent.

Ocean Model

The ocean model consists of a zonally averaged deep ocean with a uniform 4000 m depth between latitudes ϕ_N=66°N and ϕ_S=66°S. The vertical mixing processes occurring in the model are (1) vertical diffusion, (2) convective overturning, (3) thermohaline overturning, and (4) wind driven overturning. The governing equations are

Horizontal equations of motion

$$-fv=-\frac{1}{\rho r\cos\phi}\frac{\partial P}{\partial\lambda}+\frac{\partial}{\partial z}\left(A\frac{\partial u}{\partial z}\right) \tag{1}$$

$$fu=-\frac{1}{\rho r}\frac{\partial P}{\partial\phi}+\frac{\partial}{\partial z}\left(A\frac{\partial v}{\partial z}\right) \tag{2}$$

Continuity equation

$$\frac{\partial w}{\partial z}+\frac{1}{r\cos\phi\,\gamma}\frac{\partial}{\partial\phi}(v\cos\phi\,\gamma)=0 \tag{3}$$

Hydrostatic balance

$$\frac{\partial P}{\partial z}=-\rho g \tag{4}$$

Equation of state

$$\rho=\rho(T,S,P) \tag{5}$$

Temperature and salinity equations

$$\frac{\partial}{\partial t}\begin{Bmatrix}T\\S\end{Bmatrix} = -\frac{1}{r\cos\phi\,\gamma}\frac{\partial}{\partial\phi}\left(v\begin{Bmatrix}T\\S\end{Bmatrix}\cos\phi\,\gamma\right) + \frac{1}{r^2\cos\phi\,\gamma}\frac{\partial}{\partial\phi}\left(K_h\cos\phi\,\gamma\frac{\partial}{\partial\phi}\begin{Bmatrix}T\\S\end{Bmatrix}\right) - \frac{\partial}{\partial z}\left(w\begin{Bmatrix}T\\S\end{Bmatrix}\right) + \frac{\partial}{\partial z}\left(K_v\frac{\partial}{\partial z}\begin{Bmatrix}T\\S\end{Bmatrix}\right) + q^{conv} \quad (6)$$

Here u, v and w are the zonally averaged zonal, meridional and vertical velocity components; ϕ, λ, and z are latitude, longitude, and depth; ρ is density, r is the Earth's radius, γ is zonal oceanic fraction, K_h and K_v are horizontal and vertical diffusion coefficients, A is the vertical viscosity coefficient, and q^{conv} represents convective overturning. The nonlinear equation of state of *Friedrich and Levitus* [1972] is used.

In this paper we adopt a simplified geometry with a continent at all latitudes. The dynamical boundary conditions applied are: $\rho A u_z = \tau$ and $v_z = w = 0$ at the upper boundary ($z=z_2$), and $u_z = v_z = w = 0$ at the lower boundary, where τ is the fixed zonal surface wind stress.

A stream function ψ is introduced which leads to the

$$\psi_{zzzz} + \left(\frac{2A_z}{A}\right)\psi_{zzz} + \left(\frac{A_{zz}}{A}\right)\psi_{zz} + \left(\frac{f}{A}\right)^2\psi = \frac{g}{\rho A r}\frac{\partial\rho}{\partial\phi} - \frac{1}{A^2}\int_{z_1}^{z}\frac{f}{\rho r\cos\phi}\frac{\partial P}{\partial\lambda}dz \quad (7)$$

The component of the zonal pressure gradient due to density variations, $(\partial P/\partial\lambda)_i$, is parameterized in terms of the component of the meridional pressure gradient due to density variations, $(\partial P/\partial\phi)_i$, based on *Wright and Stocker* [1991] as follows:

$$\left(\frac{\partial P}{\partial\lambda}\right)_i = -2\sin\phi\cos\phi\,\varepsilon\left(\frac{\partial P}{\partial\phi}\right)_i \quad (8)$$

with $\varepsilon = 0.25$. As shown by *Harvey* [1992], this leads to the following diagnostic equations for ψ for $A \approx O(10^{-4})$ m^2 s^{-1}:

$$\psi = -\left(\frac{z-z_1}{D}\right)\frac{\tau}{\rho f} + \frac{gA}{\rho f^2 r}\frac{\partial\rho}{\partial\phi} + \frac{2\sin\phi\,\varepsilon}{\rho f r}\left(\int_{z_1}^{z}\frac{\partial P}{\partial\phi}dz - \left(\frac{z-z_1}{D}\right)\int_{z_1}^{z_2}\frac{\partial P}{\partial\phi}dz\right) \quad (9)$$

where z_1 is the lower boundary and z_2 is the upper boundary.

Whenever an unstable potential density profile occurs between any two layers, convective overturning is assumed to occur and to establish uniform temperature and salinity over the unstable depth interval. Based on *Gargett* [1984], the vertical diffusion coefficient K_v is parameterized in terms of the local Brunt-Vaisala frequency N as

$$K_v = \frac{A_0}{N}, \qquad K_{min} \le K_v \le 10^4 \text{ cm}^2\text{ s}^{-1} \quad (10)$$

where A_0 and K_{min} are specified and

$$N = \left(-\frac{g}{\rho}\frac{\partial\rho}{\partial z}\right)^{1/2} \quad (11)$$

The diffusion coefficients for heat and salt are assumed to be equal, and the vertical viscosity coefficient A is assumed to be equal to K_v (with the constraint $A_0 \le 10^{-2}$ m^2 s^{-1}). The horizontal diffusion coefficient K_h is fixed at a value of 1 x 10^3 m^2 s^{-1} below the mixed layer, but is set to $O(10^4)$ m^2 s^{-1} within the mixed layer.

An isothermal mixed layer serves as an upper boundary to the deep ocean domain. The governing equation for mixed layer temperature, in the absence of sea ice, is

$$C\frac{\partial T}{\partial t} = Q^* + L\downarrow - L\uparrow - H - L - \rho c_p K_V\frac{\partial T}{\partial z}\Big|_{z=-h} + \frac{1}{r^2\cos\phi\,\gamma}\frac{\partial}{\partial\phi}\left(C\,K_H\cos\phi\,\gamma\frac{\partial T}{\partial\phi}\right) - C\,\nabla(v,w)T + q_{conv} \quad (12)$$

where $C=\rho c_p h$ is the mixed layer thermal inertia (h=75 m is the mixed layer depth, ρ is a fixed water density of 1000 kg m^{-3} and c_p is the specific heat of water), Q^* is the solar energy flux absorbed by the mixed layer, $L\downarrow$ and $L\uparrow$ are the downward and upward infrared radiative fluxes, H and L are upward sensible and latent heat fluxes, and q_{conv} represents convective heat exchange. The remaining terms of Eq. (12) represent the effects of diffusion and advection. The computation of Q^*, $L\downarrow$, $L\uparrow$, H and L is explained by *Harvey* [1988a].

The governing equation for mixed layer salinity in the absence of sea ice is

$$h\frac{\partial S}{\partial t} = \bar{S}(P+R-E) - K_v\frac{\partial S}{\partial z}\Big|_{z=-h} + \frac{1}{r^2\cos\phi\,\gamma}\frac{\partial}{\partial\phi}\left(hK_H\cos\phi\,\gamma\frac{\partial S}{\partial\phi}\right) - h\nabla(v,w)S + q_{conv} \quad (13)$$

where q_{conv} represents the effect of convection; $\bar{S}$ is the global mean surface salinity; and P, R, and E are the precipitation, runoff, and evaporation rates, respectively. Details concerning the treatment of sea ice can be found by *Harvey* [1992].

A uniform 4° latitudinal resolution is used, while the vertical resolution increases gradually from 75 m in the upper ocean to 400 m at the ocean bottom, giving a total of 45 latitude zones and 20 deep ocean layers (plus the mixed layer).

Results

This paper begins by examining the model transient response to a step function, latitudinally uniform surface-troposphere heating perturbation ΔQ of 6 W m^{-2} which is

accompanied by an increase in downward infrared radiation at the land and ocean surface of 1 W m^{-2}. This roughly mimics the heating perturbation that might accompany a CO_2 doubling if concurrent increases in other greenhouse gases are taken into account (see *Kiehl and Ramanathan* [1982] with respect to relative heating perturbations at the tropopause and surface for a CO_2 increase). The direct effect of a GHG increase is largely to heat the troposphere, but because the troposphere and surface are tightly coupled through radiative and turbulent heat exchanges, tropospheric warming leads to a concurrent surface heating perturbation, such that the troposphere and surface tend to respond as a single system to the net surface-troposphere heating perturbation.

The behavior of the coupled atmosphere-ocean climate model is initially investigated using a globally uniform ocean fraction and hemispherically symmetric wind stress forcing of the mixed layer, and with ice and snow suppressed. Two sets of experiments are presented, one in which K_v is fixed, and one in which K_v is parameterized based on (10).

Fixed K_v Case

We begin with a series of experiments, listed in Table 1, in which K_v is fixed at values ranging from 1 x 10^{-5} m^2 s^{-1} to 5 x 10^{-4} m^2 s^{-1}. In the first four experiments the unperturbed flow field consists of a dominant thermohaline overturning cell spanning both hemispheres (see Figure 1a), with mean annual mixed layer temperature at a given latitude up to 10°C warmer in the hemisphere where downwelling occurs and the mixed layer salinity up to 6‰ higher. In the remaining two experiments the unperturbed flow, temperature, and salinity fields are close to hemispherically symmetric, with comparable overturning cells filling each hemisphere with downwelling at high latitudes and upwelling centered at the equator (Figure 1b). The magnitude of the unperturbed overturning flux for each experiment is given in Table 1. For cases with a single cell, the temperature gradient opposes the overturning and the salinity gradient drives the overturning, while in the double cell cases, the temperature gradient is the driving factor and the salinity gradient opposes the circulation.

Global mean thermal response. Figure 2 shows the globally averaged mixed layer and deep ocean transient temperature response for all experiments. One measure of the transient response time scale is the *e*-folding time, τ_e, which is the time required to reach $(1 - e^{-1}) = 0.63$ of the steady state response. For a one-box thermal reservoir, τ_e arises as the time constant in the solution to the governing equations, while for more complex models a variety of time constants arises [Harvey, 1986; Watts et al, 1994]. Nevertheless, it is useful to compare the time required to reach a given fraction of the steady state response for different ocean model versions, and because τ_e has been extensively reported by other workers, it is convenient to use it here. Values of τ_e for the mixed layer are given in Table 1.

There are two systematically changing but competing effects on the transient response timescale as K_v increases: a tendency for larger K_v to give a slower transient response, and a tendency for the increase in overturning circulation intensity as K_v increases [see Bryan, 1987] to give a faster transient response. As explained by *Harvey and Schneider* [1985], use of stronger but fixed overturning intensity causes a faster surface transient response because heating anomalies

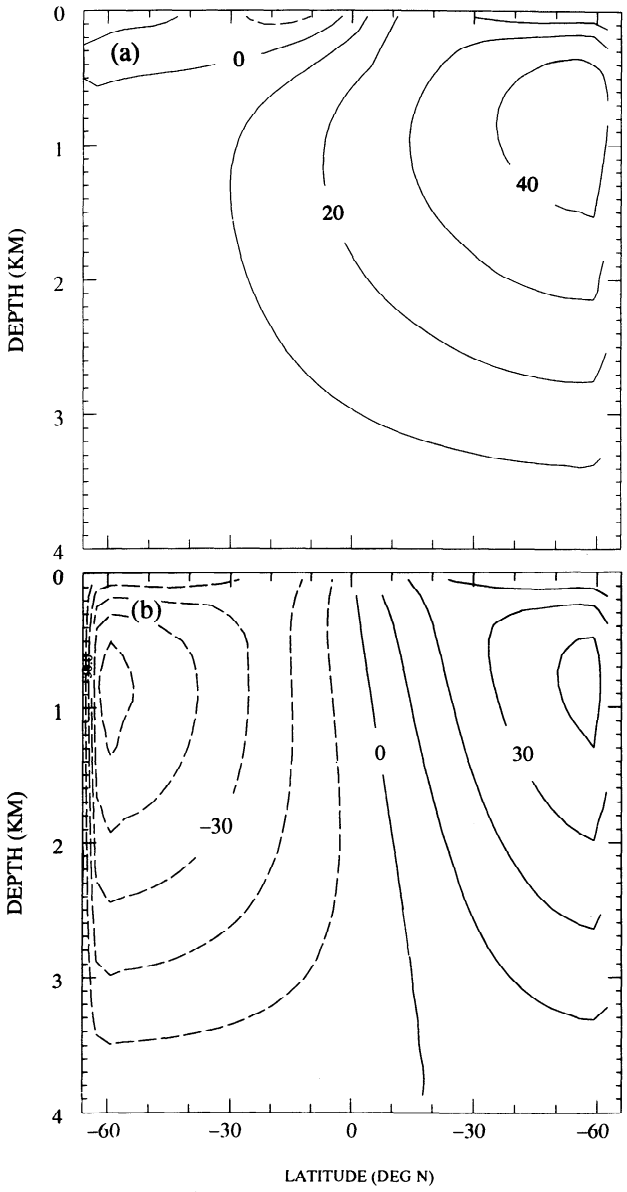

Figure 1. Steady state overturning circulation for (a) experiment SF2 (representative of experiments SF1-SF4) and (b) experiment SF5 (representative of experiments SF5-SF6) prior to a GHG increase.

Table 1. Experiments Performed With the Hemispherically Symmetric Model Version and Fixed K_v, as Well as the Nature and Magnitude of the Unperturbed Thermohaline Circulation (per Cell) and Surface Temperature *e*-Folding Response Time τ_e to a Step Function External Forcing Change

Experiment	K_v, m^2 s^{-1}	Nature of Circulation	Peak Flux, Sv	τ_e, years
SF1	1 x 10^{-5}	Single Cell	21	10
SF2	5 x 10^{-5}	Single Cell	49	18
SF3	7 x 10^{-5}	Single Cell	59	21.2
SF4	8 x 10^{-5}	Single Cell	63	20.8
SF5	1 x 10^{-4}	Two Cell	44	49
SF6	5 x 10^{-4}	Two Cell	120	142

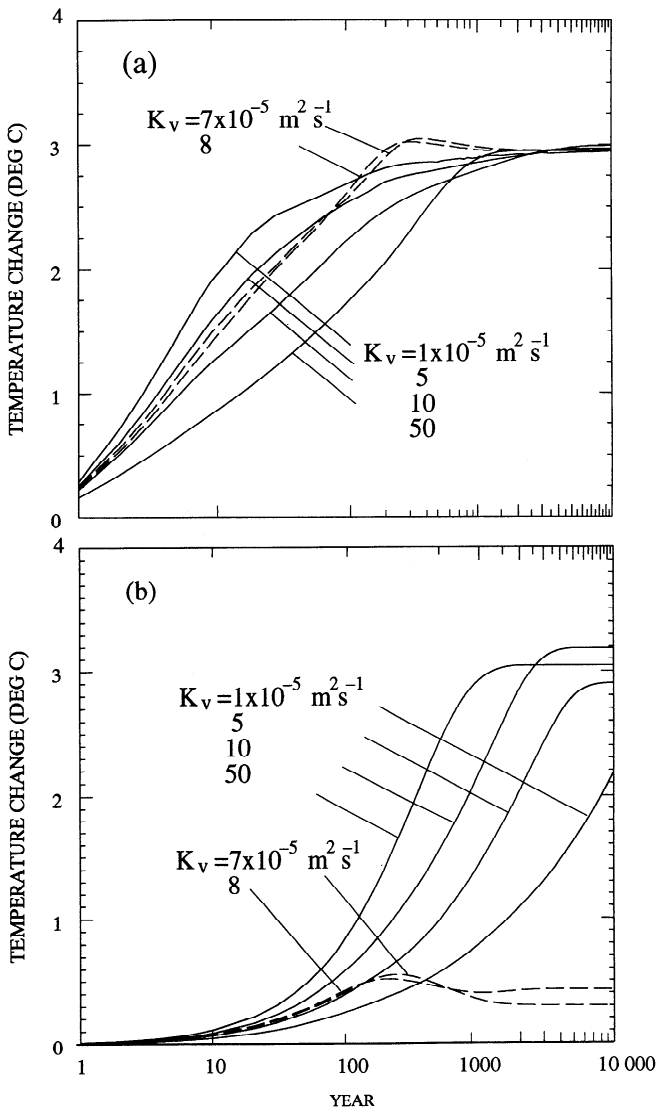

Figure 2. Globally averaged (a) mixed layer and (b) deep ocean temperature response to a step function greenhouse heating perturbation of 6 W m^{-2} using fixed K_v ranging from 1 x 10^{-5} m^2 s^{-1} to 5 x 10^{-4} m^2 s^{-1}.

which diffuse into the upper ocean are more rapidly advected back into the mixed layer when the overturning is stronger. Here the former effect dominates, such that increasing K_v tends to produce a slower surface transient response (but a faster deep ocean response). An exception occurs between experiments SF3 and SF4, in which τ_e decreases slightly as K_v is increased. This is followed by a sudden increase in τ_e as K_v increases between experiments SF4 and SF5, which coincides with the transition from a one-cell to a two-cell structure in the unperturbed state.

The reversal in the variation of τ_e with K_v and subsequent discontinuity are related to differences in the transient circulation response. As discussed below, the overturning circulation is not fixed but weakens during the transient in all experiments, and as explained by *Harvey and Schneider* [1985], such a weakening slows the surface transient response. In the perturbed steady state the overturning circulation is qualitatively similar to the unperturbed steady state in all experiments except SF3 and SF4, but is slightly stronger. In experiments SF3 and SF4, however, the heating perturbation induces a transition from a predominantly single cell to a double cell structure. During the transient the main cell weakens, which tends to slow the transient surface response, while a new cell develops from an incipient overturning cell in the opposite hemisphere (seen at latitude 10-40°S in Figure 1a) and eventually fills the entire hemisphere. As shown by *Harvey and Schneider* [1985], an increase in overturning intensity leads to a faster surface transient response. This in turn causes the comparatively fast transient response in SF3 and SF4. In experiment SF5 the unperturbed circulation already has a two-cell structure and local transient strengthening of the overturning circulation does not occur, which explains the large jump in τ_e.

It can be seen from Figure 2 that the globally averaged transient surface temperature response overshoots the steady state response in experiments SF3 and SF4. This is consistent with results obtained by *Harvey and Schneider* [1985] with a one-dimensional (1-D) model, in which a strengthening of the overturning circulation during the transient induces an overshoot of the steady state response.

Figure 3 shows the variation with depth of globally averaged ocean temperature warming in steady state (except for experiment SF1, in which steady state had not been achieved after 10,000 years). The warming is nearly uniform with depth in all experiments except SF3 and SF4, with a weak minima centered near the 500 m depth which is caused by the aforementioned slight steady state strengthening of the overturning circulation, which leads to an increase in the upwelling of cold water through most of the ocean basin. In experiments SF3 and SF4, however, the development of a second major overturning cell provides a new source of cold polar water to the deep ocean. Even though the polar regions warm, the new sinking water remains comparatively cold, thereby limiting warming of the deep ocean. Indeed, a slight cooling occurs at some depths in experiment SF3. Mean deep

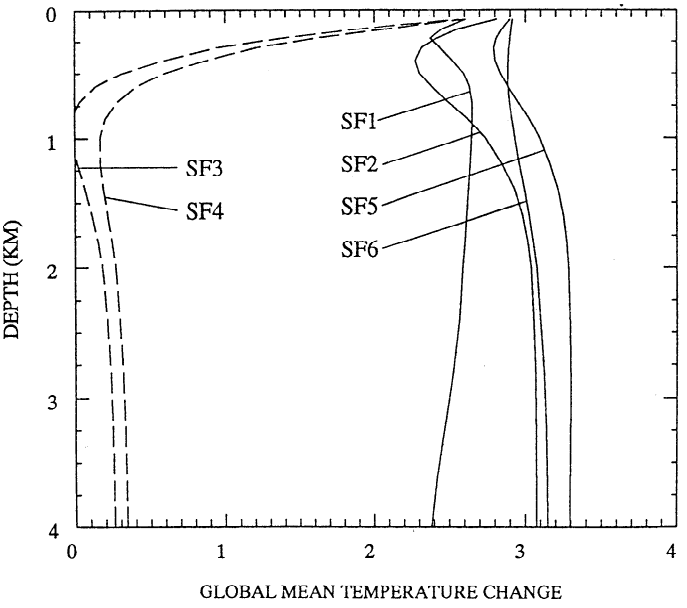

Figure 3. Vertical variation of globally averaged ocean temperature response to a GHG heating perturbation of 6 W m^{-2} for experiments SF1 to SF6. In experiment SF1 a steady state had not been achieved after 10,000 years.

ocean warming (Figure 2b) is an order of magnitude smaller than the global mean surface temperature response (Figure 2a).

Circulation response. The intensity of the main overturning cell decreases by 15-30% during the first few decades of the transient response in all experiments. A similar transient weakening of overturning is reported by *Stouffer et al.* [1989], *Washington and Meehl* [1989], and *Mikolajewicz et al.* [1990]. The decrease in overturning intensity during the initial transient response implies a transient reduction in the meridional density gradient. An initial latitudinally uniform mixed layer warming will cause a decrease in mixed layer density at low latitudes which is about 3 times larger than at high latitudes due to the nonlinear dependence of ρ on temperature. This will increase the mixed layer $\nabla\rho$. However, the reduced mixed layer density in the high latitude downwelling region will lead to a reduced meridional $\nabla\rho$ below the mixed layer as the density perturbation is advected downward, thereby reducing ∇P ($=\int \nabla\rho dz$) and causing an initial reduction of overturning. High density surface water at high latitudes is subsequently advected downward less rapidly, reducing $\nabla\rho$ below the mixed layer and further weakening the overturning circulation through a positive feedback. High-latitude convection also decreases, but the suppression of convection is not a significant factor in the partial collapse of the overturning circulation. This is confirmed by the fact that both the unperturbed circulation and the transient circulation response are almost identical for cases with and without convection permitted. Since the partial circulation collapse is dependent on downward advection of surface density anomalies, the collapse (and subsequent recovery) occur sooner with increasing K_v (which is associated with more vigorous circulation).

In experiments SF3 and SF4 the main overturning cell weakens through the process described above. Since this cell transports salt from the upwelling (northern) to downwelling (southern) hemisphere, its weakening leads to a surface salinity increase at middle latitudes in the upwelling hemisphere. This in turn causes downwelling to develop below the salinity anomaly. Similar initial transient salinity and salinity-induced circulation anomalies occur in experiments SF1 and SF2, but in the case of experiments SF3 and SF4, the salinity field and associated circulation completely reorganizes. Figure 4 shows the latitude-depth variation of the steady state change in oceanic temperature and salinity for experiment SF3; also shown is the change in stream function $\Delta\psi_T$ obtained by subtracting the initial ψ field from that obtained using the perturbed temperature field but the original salinity field; and $\Delta\psi_S$, which is based on salinity changes. The sum $\Delta\psi_T+\Delta\psi_S$ differs from the observed $\Delta\psi$ by no more than a few percent. The steady state circulation change is dominated by the change in salinity field, in contrast to the first part of the transient, where $\Delta\psi_T$ dominates the circulation change.

In all experiments except SF3 and SF4 the meridional overturning intensity increases (by up to 6%) between the unperturbed and perturbed steady states at middle and high latitudes but decreases at low latitudes, while total oceanic meridional heat flux generally changes by less than 2%, as increased advective heat flux is partly offset by decreased diffusive heat flux. To gain insight into the factors associated with these circulation changes, we show in Figure 5 the

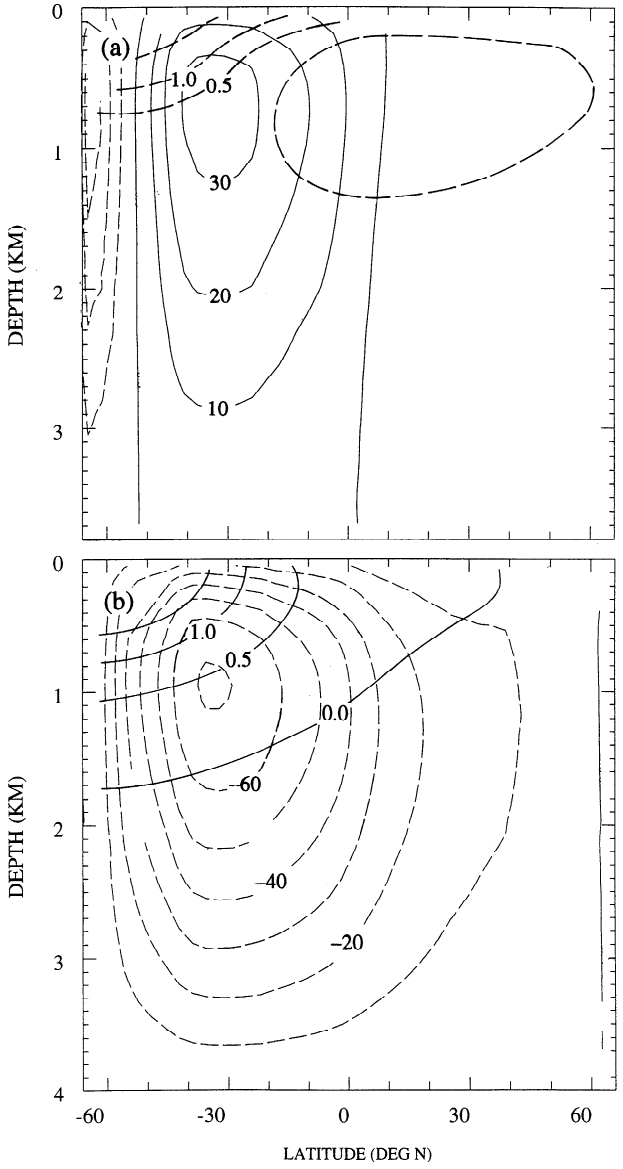

Figure 4. Results for experiment SF3: (a) Steady state deep ocean temperature change (dashed, 0.5°C contour interval) and temperature-induced stream function change (solid and dashed, 10 Sv contour interval); (b) steady state deep ocean salinity change (solid, 0.5‰ contour interval) and salinity-induced stream function change (dashed, 10 Sv contour interval).

steady state ΔT and ΔS fields for experiment SF2, along with $\Delta\psi_T$, $\Delta\psi_S$, the unperturbed flow field, and $\Delta\psi_T+\Delta\psi_S$, which differs from the observed $\Delta\psi$ by no more than a few percent. The temperature and salinity changes alone produce large but opposing circulation changes which locally overwhelm the unperturbed circulation. The net circulation change is a small residual in SF2, which suggests that the magnitude and direction of the net change is sensitive to small relative errors in the temperature- and salinity-change fields.

Comparing the steady state $\Delta\psi_T$ and $\Delta\psi_S$ fields for experiments SF3 (Figure 4) and SF2 (Figure 5), we see that, whether there is little change in the circulation in the new steady state or a complete reorganization, the temperature

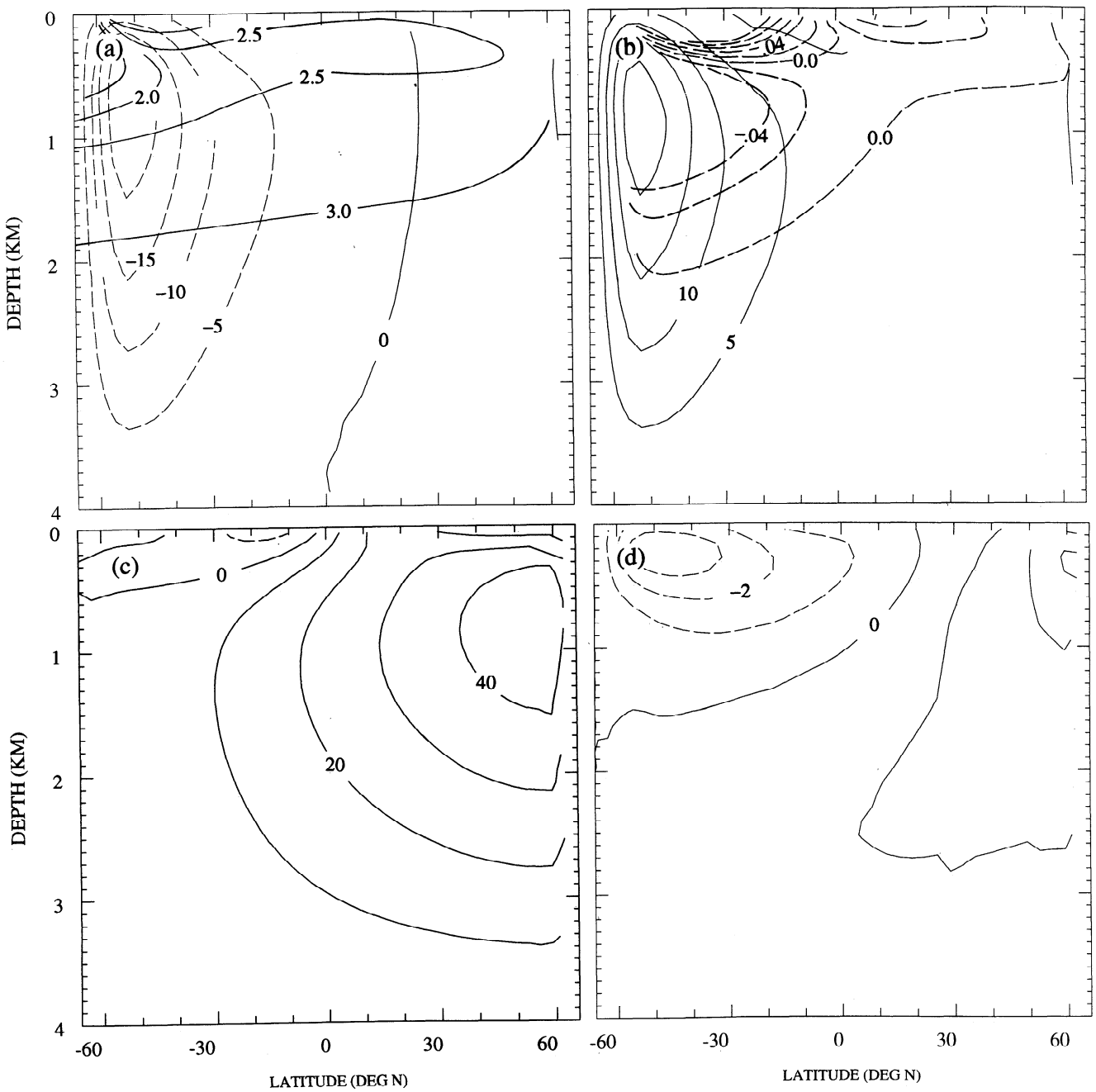

Figure 5. Results for experiment SF2: (a) Steady state deep ocean temperature change (solid, 0.5°C contour interval) and temperature-induced stream function change (solid and dashed, 5 Sv contour interval); (b) steady state deep ocean salinity change (dashed, 0.02‰ contour interval) and salinity-induced stream function change (solid, 5 Sv contour interval); (c) unperturbed flow field; and (d) total stream function change.

and salinity changes alone induce large circulation changes. The difference is that in one case these perturbations almost perfectly cancel, whereas in the other case they do not.

Manabe and Bryan [1985] note a slight increase in thermohaline overturning intensity as their model climate warms. They attribute this near-constancy to compensation between greater warming at high latitudes, which would tend to decrease the overturning intensity, and the nonlinear nature of the equation of state, such that the thermal expansion of seawater per degree of warming is smaller at low than at high temperatures, and is thus smaller at high than at low latitudes. The analysis presented here indicates that temperature changes alone produce a significant weakening of the overturning circulation, and that near constancy is a result of compensation between temperature and salinity-induced changes. Further analysis of the response in GCMs seems to be warranted.

When a heating perturbation of 10 W m^{-2} is applied, the response is similar to that obtained using 6 W m^{-2}, except that the transition from a single cell to a two-cell structure is

induced at a smaller value of K_v. The model circulation regime depends, among other factors, on the value of K_v and absolute ocean temperature. At larger temperatures the impact of a given temperature gradient on the density gradient is larger. Since the salinity gradient drives the circulation in the one-cell regime and the temperature gradient opposes it, an overall warming can induce a transition from a one-cell to a two-cell regime if the value of K_v is such that the model is already close to the boundary between the two regimes. The further the model is from the boundary (the smaller K_v) the larger the temperature warming needed to induce the transition.

Latitudinal variation in response. Figure 6 shows the latitudinal variation of atmospheric temperature response for experiments SF2 and SF6 (corresponding to K_v values of 5 x 10^{-5} m^2 s^{-1} and 5 x 10^{-4} m^2 s^{-1}, respectively). As noted above, the overturning circulation weakens during the transient. Since the overturning circulation induces a net upward heat flux to the mixed layer and a poleward heat flux to the region of downwelling [see Harvey, 1992, Figure 10b], a weakening of the overturning circulation leads to a significantly slower high latitude temperature response in one hemisphere (one cell case, Figure 6a) or in both hemispheres (two-cell case, Figure 6b). However, the latitudinal variation of steady state mixed layer temperature change is almost identical in these two experiments (and all others except SF3 and SF4), increasing from 2.8°C at the equator to 3.3°C near the poles, in spite of the very different initial flow and

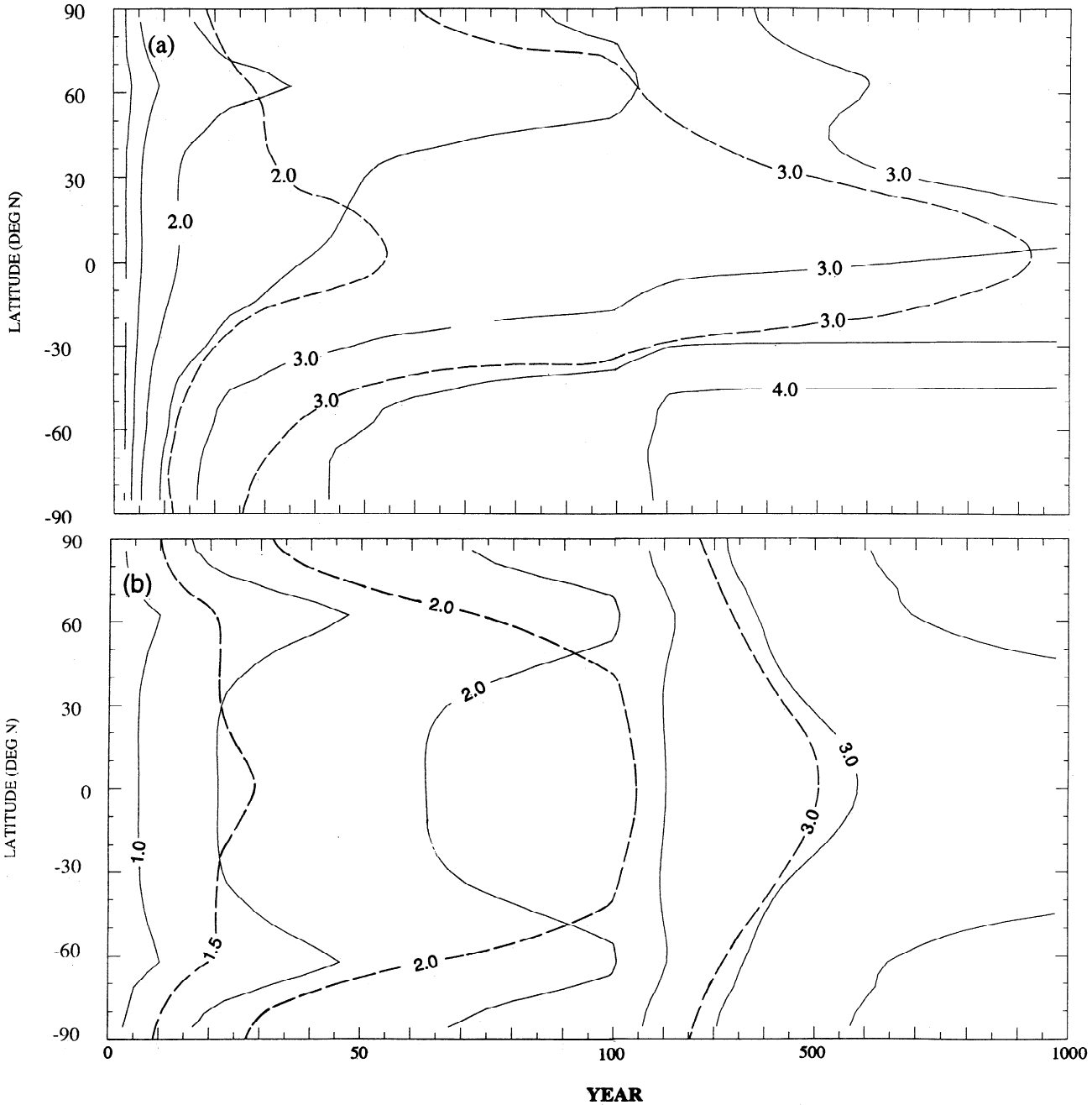

Figure 6. Latitude-year variation of atmospheric temperature for (a) experiment SF2 (K_v = 5 x 10^{-5} m^2 s^{-1}) and (b) SF6 (K_v = 5 x 10^{-4} m^2 s^{-1}). The broken lines show responses when the circulation is frozen at the unperturbed flow during the transient. Note the change in timescale at 100 years.

temperature fields for the two circulation regimes. In experiments SF3 and SF4, the development of a second strong overturning cell in the southern hemisphere (SH) accelerates the transient warming at middle and high latitudes in the SH. Since the original, interhemispheric overturning cell is permanently weakened, steady state warming in the northern hemisphere is suppressed (to about 1°C at 60°N) but enhanced in the SH (to about 8°C at 60°S). In summary, the steady state latitudinal surface temperature change, in the absence of ice and snow feedback, is close to uniform with latitude if the circulation is unchanged, and hence is similar for cases having qualitatively different initial circulation regimes. Steady state and transient circulation changes, however, have a significant effect on surface temperature changes, with local suppression of warming where the overturning circulation weakens and local enhancement where the circulation strengthens or where a new overturning cell develops.

The above mentioned delay in high-latitude warming occurs in regions where strong downwelling occurs. *Manabe et al.* [1991] attributed the delay in surface warming in regions of downwelling obtained in their model to the larger effective surface thermal inertia due to downward mixing. One can assess the relative importance of greater effective thermal inertia and decreased meridional heat flux in causing a delay in high-latitude warming here by preventing the overturning circulation from changing once the GHG increase is applied. This was done for experiments SF2 and SF6, and results are compared with the case in which the circulation is allowed to change in Figure 6. When the circulation is frozen, a 2°C warming occurs sooner at high latitudes than at low latitudes as a result of the relatively shallow (100 m depth) shelf which occurs poleward of the deep ocean. When the circulation is allowed to weaken the 2°C high-latitude warming is substantially delayed. Later, as the circulation reintensifies, the difference between frozen and unfrozen circulation cases decreases. Hence in the present model, reduced poleward heat flux rather than a greater effective high-latitude thermal inertia is the dominant factor in causing slower high-latitude temperature response to a heating perturbation.

Thermal damping. Figure 7 shows the variation of globally averaged surface+atmosphere thermal damping for experiments SF2 and SF6. This consists of (1) the increase in net radiative emission to space as a result of surface and atmospheric temperature increases (and associated radiative feedback processes); and (2) the increase in heat flux from the ocean mixed layer to the deep ocean. The difference between the sum of these flux changes and the external forcing change (6 W m^{-2}) gives the rate of change of globally averaged surface+atmosphere heat content. Because the mixed layer warms faster than deeper ocean layers, the downward diffusive heat flux increases and the upward convective heat flux decreases during the transient. As K_v, ocean circulation intensity, and absolute mixed layer-deep ocean heat fluxes increase in going from experiments SF2 to SF6, the peak ocean heat flux damping also increases, from almost 1/2 the external forcing in experiment SF2 to about 2/3 the external forcing in experiment SF6. This in turn produces a slower surface transient response as K_v increases.

Table 2 compares the individual components of the heat flux from the mixed layer to the deep ocean for the unperturbed steady state for experiments SF2 and SF6, as well as

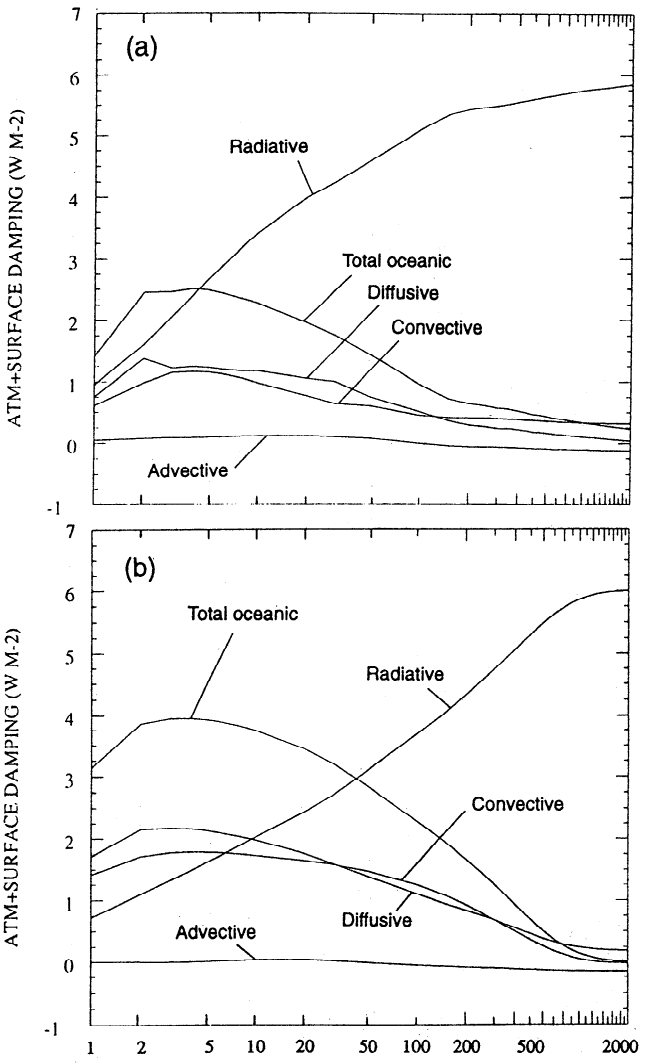

Figure 7. Variation of global mean radiative damping and perturbation in mixed layer-to-deep ocean heat flux for (a) experiment SF2 (K_v = 5 x 10^{-5} m^2 s^{-1}) and (b) experiment SF6 (K_v = 5 x 10^{-4} m^2 s^{-1}).

the steady state changes in these fluxes following the external forcing change. Because the mixed layer warms more than deeper layers both during the transient and in steady state, the downward diffusive heat flux increases at all times. However, the change in net heat flux to the deep ocean must be zero in steady state, which requires that the convective and/or advective upward heat fluxes increase in steady state. Since advection produces a net upward heat transport, the increase in overturning intensity leads to increased upward heat transport, as expected. The small increase in upward convective heat flux is unexpected, given the greater warming of the mixed layer than underlying layers; it is the result of an expansion in the areal extent of convection by one grid point due to changes in the salinity field which more than offsets a decrease in convective heat flux everywhere else.

Role of convection. Figure 8 compares the global mean mixed layer response for experiments SF2, SF5, and SF6 using model versions with and without convection. The occurrence of convection increases the time required to reach

Table 2. Heat Fluxes From the Mixed Layer to Deep Ocean Averaged Over the Global Ocean for the Unperturbed Steady State for Experiments SF2 and SF6, and Changes in These Fluxes in the Perturbed Steady State

Experiment	Flux	Unperturbed Value, W m^{-2}	Change, W m^{-2}
SF2	Convective	-9.52	-0.15
SF2	Diffusive	11.27	0.77
SF2	Advective	-1.91	-0.47
SF6	Convective	-25.62	-0.05
SF6	Diffusive	30.41	0.29
SF6	Advective	-4.79	-0.23

a 1°C global mean warming by 20% for experiment SF2 and by 40% for experiments SF5 and SF6, with a diminishing lag for larger temperature changes. The response at any given time is up to about 10% greater in the absence of convection than in its presence. The surface temperature change in the absence of convection is greater at all times than in the presence of convection, which implies that the integrated net radiation and hence global mean deep ocean warming will be smaller in steady state, which is indeed the case.

Henderson-Sellers [1987] suggested on the basis of one-dimensional model results that inclusion of convective mixing would reduce the warming after a given time by up to a factor of 3 compared to the case without convection. The impact of convection obtained here is substantially smaller than obtained by *Henderson-Sellers* [1987] for two reasons: First, convection transports heat upward to the mixed layer, and a reduction in convection as the mixed layer warms reduces this upward heat transport, thereby having a damping effect on mixed layer temperature response. However, the transient weakening of the overturning circulation, discussed above, is less pronounced when convection is present than in its absence. Since the transient circulation weakening also has a damping effect on mixed layer temperature response, a smaller weakening of the circulation partly counteracts the direct damping effect of weaker convection. Second, convection tends to occur in regions where strong downwelling (10^2 m yr^{-1} and larger) also occurs, so that even in the absence of convection, thermal anomalies penetrate deeply. *Henderson-Sellers* [1987], on the other hand, assessed the impact of convection in a box-diffusion model which lacked advective mixing.

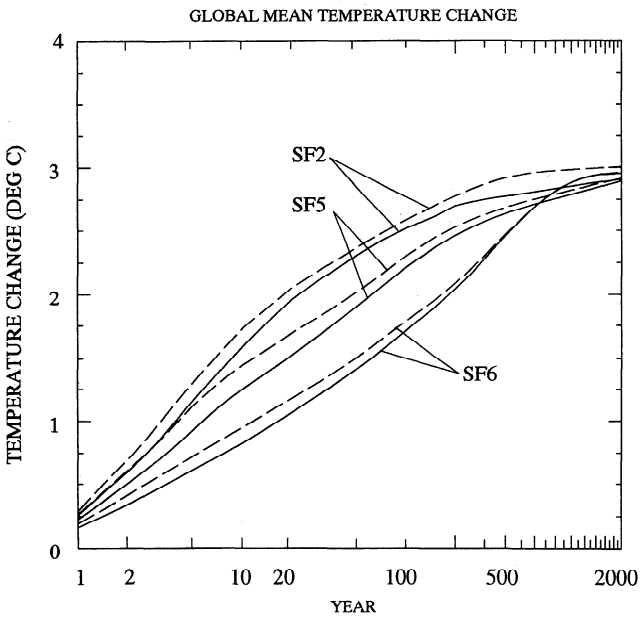

Figure 8. Global mean mixed layer temperature response for experiments SF2, SF5, and SF6 for model versions with (solid lines) and without (dashed lines) convection.

Comparison With 1-D Models

To determine the ability of the one-dimensional upwelling-diffusion model to mimic the results of the two-dimensional (2-D) model, the vertical variation of upwelling velocity (averaged over the upwelling region) obtained by the two-dimensional model for each experiment, along with the corresponding value of K_v, was used in the one-dimensional model of *Harvey and Schneider* [1985]. Three versions of the 1-D model are considered: an upwelling-diffusion version in which the temperature at which bottom water forms in polar regions is fixed as global mean mixed layer temperature increases (UD_0); an upwelling-diffusion version in which the temperature of bottom water formation is assumed to warm at the same rate as the global mean mixed layer (UD_1); and a pure-diffusion version, obtained by setting the upwelling velocity to zero (PD). Both the PD and UD_1 models produce a steady state deep ocean warming which is uniform with depth and thus is similar to that obtained with the 2-D model for all experiments except SF3 and SF4, whereas the UD_0 deep ocean warming decreases exponentially with depth and roughly matches that obtained in experiments SF3 and SF4. As discussed by *Harvey and Schneider* [1985], the surface transient response of the 1-D model is fastest for the UD_0 version because the integrated deep ocean warming is smallest, and is slowest for the UD_1 version, in which surface warming is immediately transmitted to the ocean bottom through the implicit polar downwelling. Two versions of the 2-D model are considered: the base case version, and a version in which convection is turned off.

Table 3 compares *e*-folding times for experiments SF1, SF2, SF5, and SF6. In every case the transient response of all three 1-D models is substantially faster than that of the corresponding 2-D model. This is also true in every case except one when convection is omitted (suppression of Ekman overturning cells has a negligible effect on the transient response). Representative results are given in Figure

Table 3. Comparison of Atmospheric Global Mean *e*-Folding Response Times τ_e for Alternative Versions of the One-Dimensional and Two-Dimensional Ocean Model

Experiment	2-D Model		1-D Model		
	Base	No Convection	UD_0	UD_1	PD
SF1	8.6	6.0	3	3	3
SF2	16	12.5	6	8	7
SF5	34	25	9	18	11
SF6	140	100	28	123	44

9, which compares the globally averaged (land+ocean) atmospheric temperature response of the 1-D and 2-D models for experiment SF5 (K_v = 1 x 10^{-4} m^2 s^{-1}).

The differences between the 1-D and 2-D models are a result of the transient weakening of the overturning circulation which occurs in the 2-D model, and the effect this has on advective damping. The overturning circulation heats the mixed layer, since downwelling water is colder than upwelling water. During the transient the water leaving the mixed layer warms more than the subsurface water which is advected back into the mixed layer, which reduces advective heating of the mixed layer in both the 2-D and UD_1 models. However, this damping effect is weak. A stronger damping occurs in the 2-D model but not in the 1-D model through the transient weakening of the overturning circulation. In UD_0 the temperature at which water leaves the mixed layer is constant, while the upwelling water warms, such that absolute advective heating steadily increases during the transient to an extra 1.2 W m^{-2} in steady state, giving the fastest 1-D model transient response. The development of a second strong overturning cell in experiments SF3 and SF4, and the associated transient heating effect, does not become important until after 100 years, whereas the weakening of the original overturning cell and the associated cooling effect begins immediately. For this reason the 1-D models are initially faster than the 2-D model even in experiments SF3 and SF4.

Figure 10 compares the deep ocean temperature changes at years 100, 500, and 3000 for the UD_1 and PD models with that of the 2-D model for experiment SF5. The differences between the UD_1 and 2-D model warming profiles are largely a result of the transient weakening of thermohaline overturning (by about 25%) in the 2-D model. As advection weakens, the warming anomaly penetrates more deeply into the upper ocean as a result of diffusion, giving greater upper ocean warming in the 2-D model than in UD_1, while at the same time the warming at high latitudes is carried to abyssal depths less rapidly, giving smaller deep ocean warming. The transient deep ocean warming profile obtained with the 2-D model, as well as the transient surface temperature response, can be closely replicated with the 1-D model if the overall pattern of transient upwelling changes occurring in the 2-D model is imposed in the 1-D model.

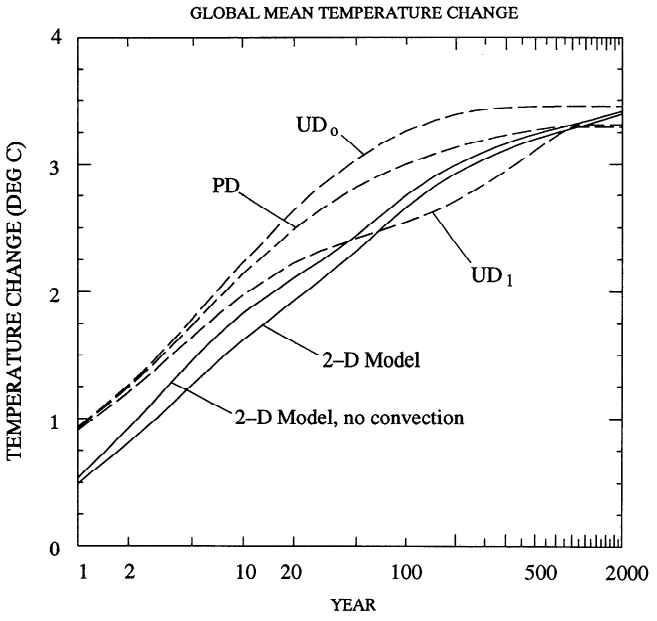

Figure 9. Globally averaged mixed layer temperature response for the 2-D ocean model using fixed K_v with and without convection and for the PD, UD_0, and UD_1 versions of the 1-D model (see text for definitions). Results are given for K_v = 1 x 10^{-4} m^2 s^{-1} (experiment SF5).

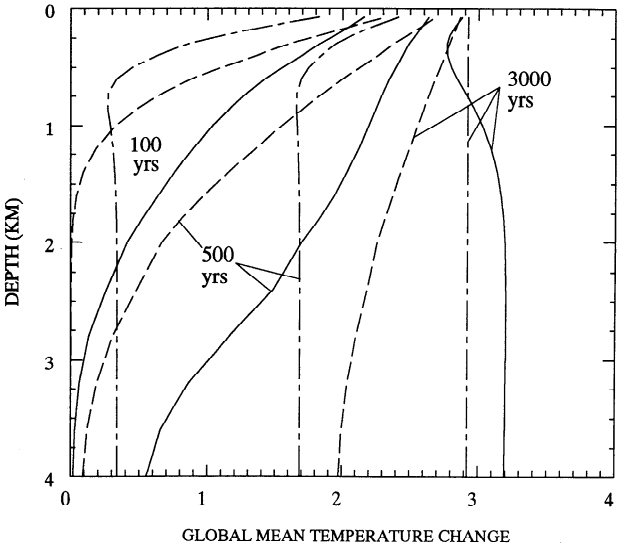

Figure 10. Globally averaged deep ocean temperature change profile (solid curves) at 100, 500, and 3000 years after a step function GHG increase for experiment SF5 (K_v = 1 x 10^{-4} m^2 s^{-1}). The dashed and dash-dot curves show profiles using the 1-D PD and UD_1 ocean models, respectively.

The PD 1-D model has been extensively used in estimating the effect of the oceans in delaying the global mean warming due to GHG increases [i.e. Wigley and Raper, 1990]. As noted above, the PD model response is significantly faster than that of the 2-D model. The realized warming 20 years after a step function GHG increase using the PD model ranges from 5% greater than that of the 2-D model for small K_v (experiment SF1) to 40% greater for large K_v (experiment SF6). The UD_1 version of the 1-D model comes closest to replicating the surface transient response of the 2-D model obtained here, even in experiments SF3 and SF4.

Variable K_v Case

In the second set of experiments, K_v is parameterized using (10) with A_0 ranging from 1 x 10^{-7} m^2 s^{-2} to 5 x 10^{-7} m^2 s^{-2}. This parameterization produces K_v values ranging from 0.15-0.20 cm^2 s^{-1} near the surface at low latitudes, to 8-150 cm^2 s^{-1} near the ocean bottom and up to an upper limit of 10^4 cm^2 s^{-1} where convective overturning occurs. In order to investigate a wide range of dynamical responses to GHG increases, experiments are performed for heating perturbations ΔQ of 6 W m^{-2} and 10 W m^{-2} using (1) latitudinally uniform precipitation, (2) hemispherically symmetric precipitation, and (3) the observed precipitation pattern. Table 4 lists the set of experiments performed. Although the first two precipitation assumptions are not realistic, they can be justified on the grounds that, first, the model contains

Table 4. Experiments Performed With the Hemispherically Symmetric Model Version and Parameterized K_v, as Well as the Nature and Magnitude of the Unperturbed Thermohaline Circulation (per Cell)

Experiment	A_o, $m^2 s^{-2}$	Nature of Circulation	Peak Flux, Sv
	With Uniform Precipitation		
SVU1	1.5×10^{-7}	One-cell	41
SVU2	2.0×10^{-7}	One-cell	49
SVU3	2.5×10^{-7}	One-cell	57
SVU4	3.0×10^{-7}	One-cell	64
SVU5	4.0×10^{-7}	One-cell	74
	With Hemispherically Symmetric Precipitation		
SVS1	1.0×10^{-7}	One-cell	38
SVS2	2.0×10^{-7}	One-cell	56
SVS3	3.0×10^{-7}	One-cell	70
SVS4	4.0×10^{-7}	Two-cell	55
	With Observed Precipitation		
SVO1	1.0×10^{-7}	One-cell	38
SVO2	2.0×10^{-7}	One-cell	50
SVO3	3.0×10^{-7}	One-cell	56
SVO4	4.0×10^{-7}	Two-cell	63
SVO5	5.0×10^{-7}	Two-cell	72

many other idealizations that may constrain the qualitative nature of its response to heating perturbations for a given precipitation field; second, comparison of results using three dramatically different precipitation patterns allows determination of those results which are independent of, or dependent on, the precipitation pattern; and third, insights can be gained in analyzing a wide range of responses that could very well be helpful in analyzing the behaviour of the present ocean model when coupled to an atmospheric model in which precipitation is freely predicted or in analyzing the behavior of coupled A/O GCMs. This modeling philosophy is vindicated by the insight into the two-dimensional model response with fixed K_v, particularly experiments SF3 and SF4, afforded by the idealistic experiments performed by *Harvey and Schneider* [1985] with a one-dimensional model, as discussed in the preceding section.

With uniform precipitation, the unperturbed circulation consists of a single overturning cell spanning both hemispheres for all experiments, which resembles the circulation in the Atlantic Ocean. With either observed or hemispherically symmetric precipitation, a single overturning cell which spans both hemispheres also occurs for $A_0 = 1 - 3 \times 10^{-7}$ m^2 s^{-2}, but roughly symmetric overturning cells, one in each hemisphere, occur for $A_0 = 4\text{-}5 \times 10^{-7}$ m^2 s^{-2}.

Figure 11 shows the variation of overturning intensity for $\Delta Q = 6$ W m^{-2} (solid lines) for all experiments using all three precipitation fields, and for $\Delta Q = 10$ W m^{-2} (dashed lines) for selected experiments (all intensities have been normalized to a value of 1.0 at year 0). For all precipitation fields, a step function GHG increase induces a transient circulation weakening, with the weakening being greater and its duration longer with smaller A_0. The circulation weakening is only weakly or not at all dependent on the magnitude of the heating perturbation for the range of perturbations considered here. With uniform precipitation the circulation weakens by about 80% during the first 100 years of the transient using

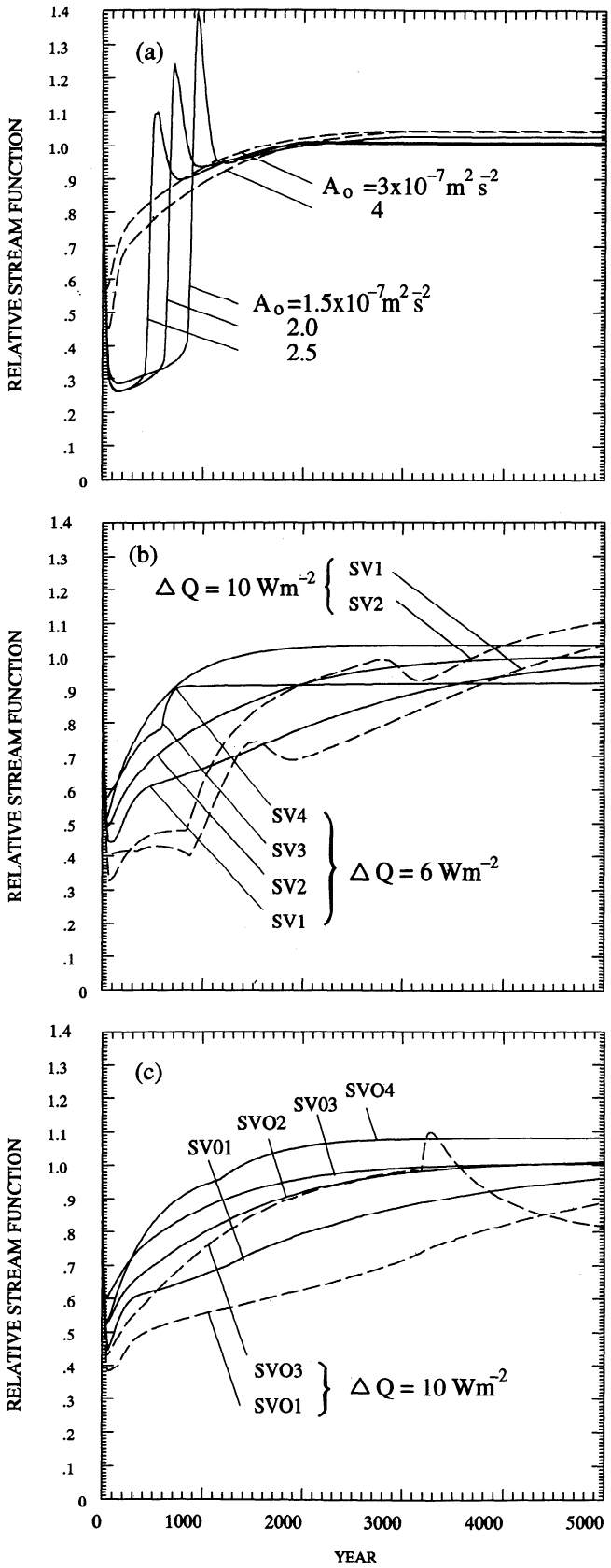

Figure 11. Variation of maximum stream function value following a step function GHG heating perturbation of 6 W m^{-2} (solid curves) or 10 W m^{-2} (dashed curves) for parameterized K_v using (a) uniform precipitation, (b) hemispherically symmetric precipitation, and (c) observed precipitation.

small A_0. This is followed by a pulse of intense overturning of 100 to 200 years duration beginning 500 to 800 years after the GHG perturbation.

Using either symmetric or observed precipitation patterns, a reduction in the overturning intensity of 45-55% occurs for ΔQ = 6 W m^{-2} and 45-65% occurs for ΔQ = 10 W m^{-2} during the first 100 years of the transient response. This weakening is larger than the weakening using fixed K_v (15-30%) and could be related to the fact that K_v in the upper ocean decreases during the early transient by about 20% when K_v is stability-dependent. The single overturning cell which occurs in the unperturbed steady state for experiments SVS1 and SVS2 (which use symmetric precipitation) is reestablished in the new steady state for ΔQ = 6 W m^{-2}, but for ΔQ = 10 W m^{-2}, the circulation which emerges after the transient collapse rotates in the opposite sense to the initial overturning cell. This circulation reversal does not occur if the observed, asymmetric precipitation pattern is used. In experiment SVS3, the unperturbed circulation also consists of a single overturning cell spanning both hemispheres, but the circulation that emerges after the transient collapse consists of two roughly symmetric overturning cells, one in each hemisphere. This response, which occurs using either a symmetric or observed precipitation pattern, is similar to the response in experiments SF3 and SF4, discussed above. The model state in experiment SVS3 is sufficiently far from the boundary between one- and two-cell circulation regimes that ΔQ = 6 W m^{-2} is not sufficient to induce the transition, whereas in experiment SVO3 (using the observed precipitation field) the model state is such that either perturbation is sufficient to induce the transition.

These circulation changes result in dramatically different variations of steady state surface temperature response with latitude, as illustrated in Figure 12. In cases in which there is no qualitative difference in the steady state circulation pattern before and after the heating perturbation, the surface transient response is relatively uniform with latitude (as illustrated by cases SVO3.Q6 and SVO4.Q10; the suffix in the preceding designator indicates the heating perturbation). The transition from a single cell to a double cell overturning pattern depresses the warming at high latitudes in the hemisphere where downwelling had exclusively occurred and enhances the warming at high latitudes in the hemisphere where a new cell is established (cases SVS3.Q6 and SVO3.-Q10 in Figure 12). The latitudinal variation of steady state response is even more marked if a complete reversal in overturning occurs (case SVS2.Q10 in Figure 12). Note that, because the transition to a two-cell structure occurs between ΔQ = 6 W m^{-2} and ΔQ = 10 W m^{-2} for case SVO3, the regional response to increasing ΔQ is highly nonlinear: at 60°N the steady state response to an increase in ΔQ from 6 W m^{-2} to 10 W m^{-2} is less than 1°C, whereas at 60°S the response is greater than 6°C.

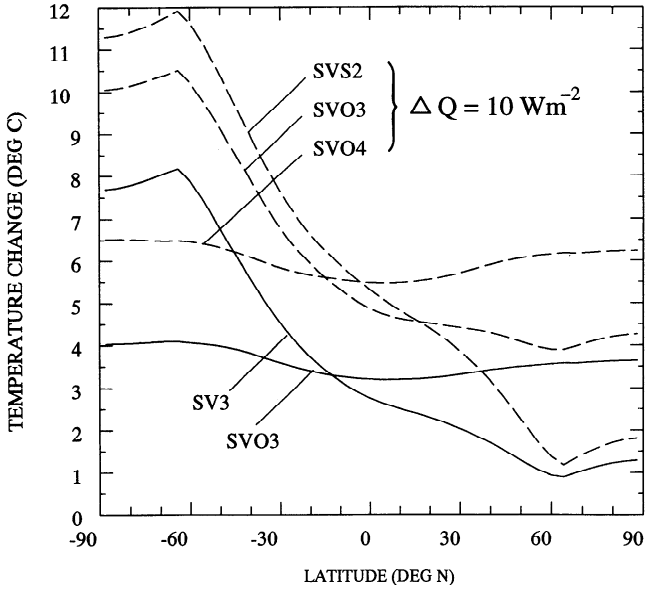

Figure 12. Latitudinal variation of steady state, zonally averaged surface temperature response for selected experiments. The suffix indicates whether a 6 W m^{-2} (.Q6) or 10 W m^{-2} (.Q10) heating perturbation was applied.

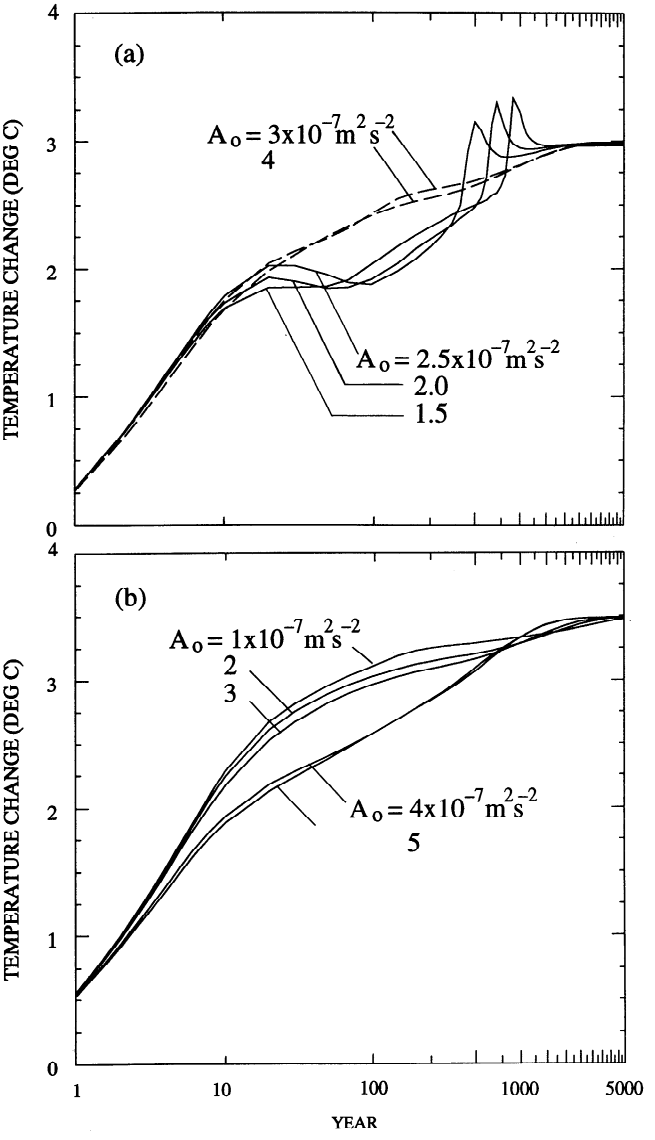

Figure 13. Globally averaged mixed layer temperature response to a step function GHG heating perturbation of 6 W m^{-2} for parameterized K_v using (a) latitudinally uniform precipitation and (b) observed precipitation.

Figure 13 shows the transient mixed layer temperature response for selected experiments, while Figure 14 shows the latitude-time variation of atmospheric temperature response for experiments SVU2.Q6 and SVO3.Q10. The near collapse of the overturning circulation during the first few decades of the transient response in experiment SVU1-SVU3 reduces both the meridional heat flux to the sinking region and global mean advective heating of the mixed layer. This causes the initial global mean surface warming to be followed by decreasing or constant surface temperature between years 20-100 of the transient response (Figure 13a) and causes initial warming of 1.5°C at high NH latitudes to be replaced by an absolute cooling in excess of 1.5°C by year 100 (Figure 14a). The subsequent intensification of overturning leads to a globally averaged heat flux from the deep ocean to the mixed layer which peaks at 1 W m^{-2}, causing renewed surface warming (and concurrent cooling of the deep ocean) to values in excess of the steady state response at high latitudes. The vigorous lateral mixing associated with the intense overturning eventually reduces meridional density gradients, leading to a reduction of overturning and net heat flux to the mixed layer and a relaxation of surface temperature back to the steady state response. In experiment SVO3.-Q10 a circulation reorganization and local regional overshoot

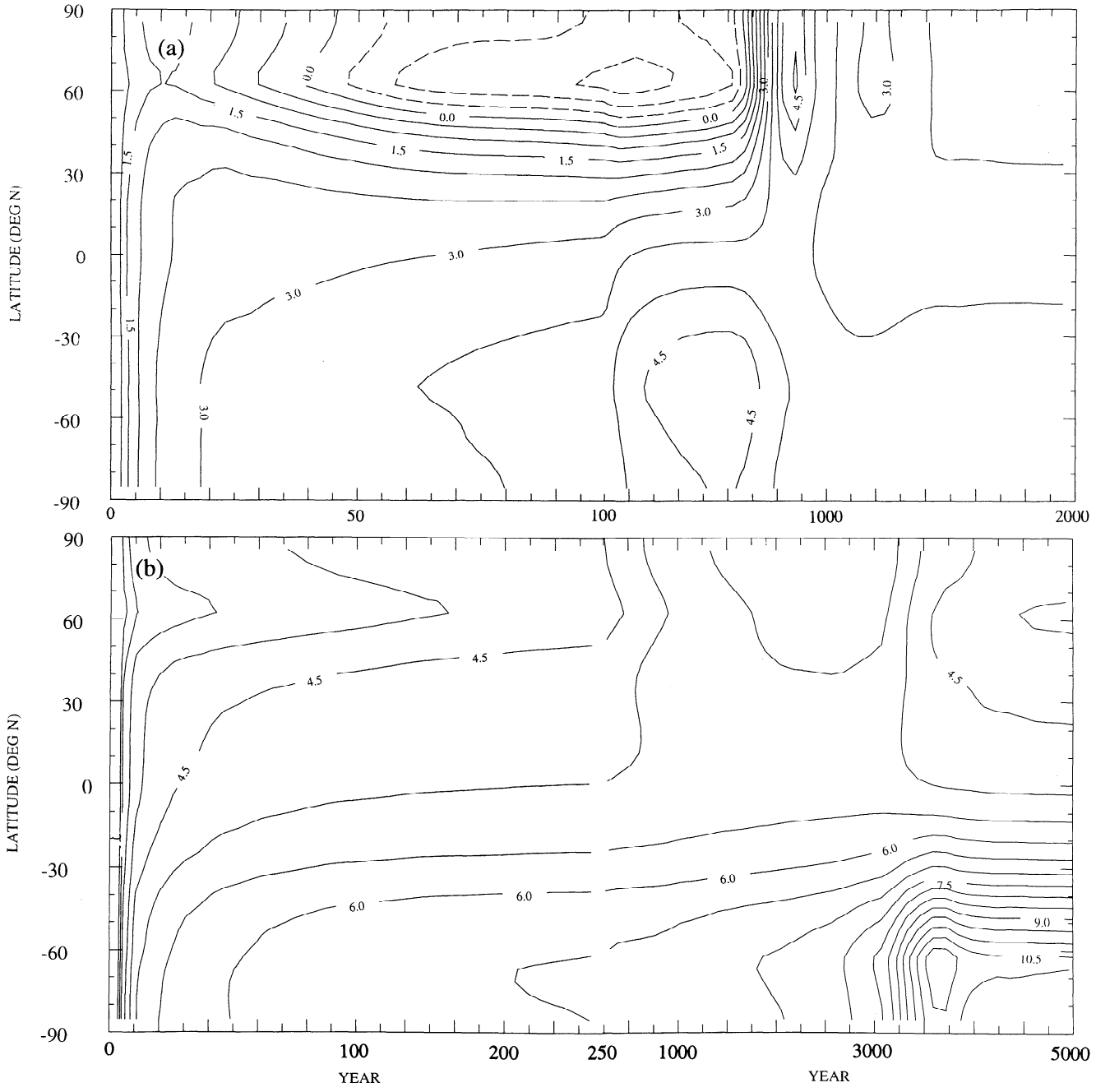

Figure 14. Latitude-year variation of atmospheric temperature response for (a) experiment SVU2 (uniform precipitation with ΔQ = 6 W m^{-2}) and (b) experiment SVO3.Q10 (observed precipatation with ΔQ = 10 W m^{-2}).

of the steady state response do not occur until 4000 years after the heating perturbation (see Figure 14b), which illustrates the very long time lags that can be associated with the model response to an external forcing change.

Figure 13b indicates that the surface transient response is substantially slower for experiments SVO4 and SVO5, both of which have two overturning cells in the unperturbed state, than for experiments SVO1-SVO3, all which have one overturning cell. The resultant discontinuity in τ_e (which jumps from 11 years in experiment SVO3 to 22 years in experiment SVO4) is similar to the discontinuity seen with fixed K_v, between experiments SF4 and SF5. However, the causal factors are different. Experiments in which the overturning circulation is frozen during the transient response indicate that the slow response for the two-cell cases is largely due to the fact that the initial weakening of the overturning circulation is greater with a two-cell regime than with a one-cell regime (see Figure 11c).

Although the uniform precipitation field used in experiments SVU1 to SVU5 is unrealistic, the extreme circulation response obtained with small A_0 could occur with more realistic fields in more highly resolved models, in which, for example, changes in net atmospheric freshwater flow between the Atlantic and Pacific basins can occur. Experiments SVU1 to SVU3 can be regarded as an analog for cases where a near total transient circulation collapse occurs and demonstrate the potential for regional reversals in the transient temperature response and overshoots of the steady state response if large enough ocean circulation changes occur. Furthermore, because these experiments represent an extreme response, their analysis yields a number of insights into the dynamics of the model behavior, as discussed below.

First, the near total circulation collapse in experiments SVU1-SVU3 causes the greatest transient warming in the global mean to occur several hundred meters below the mixed layer. This is illustrated in Figure 15 for experiment SVU2.Q6, where the warming at the 500 m depth is twice the global mean surface warming by year 600. Later, when the circulation reintensifies, heat is transferred back to the mixed layer and transient cooling occurs in the upper ocean.

Second, a comparison of experiments SVU3 (having high-latitude cooling) and SVU4 (lacking high-latitude cooling) indicates that high-latitude cooling is not compensated by faster low latitude warming. Inasmuch as the transient high-latitude cooling seen in experiments SVU1 to SVU3 is a result of reduced meridional heat advection, one might expect faster low-latitude warming for cases with high-latitude cooling than for cases without. However, the main heat redistribution is vertical instead of horizontal, as is evident from the occurrence of maximum transient deep ocean warming at 500 m depth (Figure 15).

Third, as discussed in the previous section, the initial partial circulation collapse following a GHG increase is a result of a positive feedback between the circulation and density anomalies. One might therefore expect the transient high-latitude mixed layer cooling in the downwelling region to reverse the circulation collapse in experiments SVU1-SVU3. However, comparison of Figures 11a and 14a indicates that the circulation continues to weaken after high-latitude cooling occurs. Examination of the $\Delta\psi_T$ and $\Delta\psi_S$ fields for year 100 indicates that temperature changes alone induce a vigorous overturning cell at high latitudes, with upwelling next to the boundary, which opposes the unperturbed circulation. This induced cell is twice as strong as the

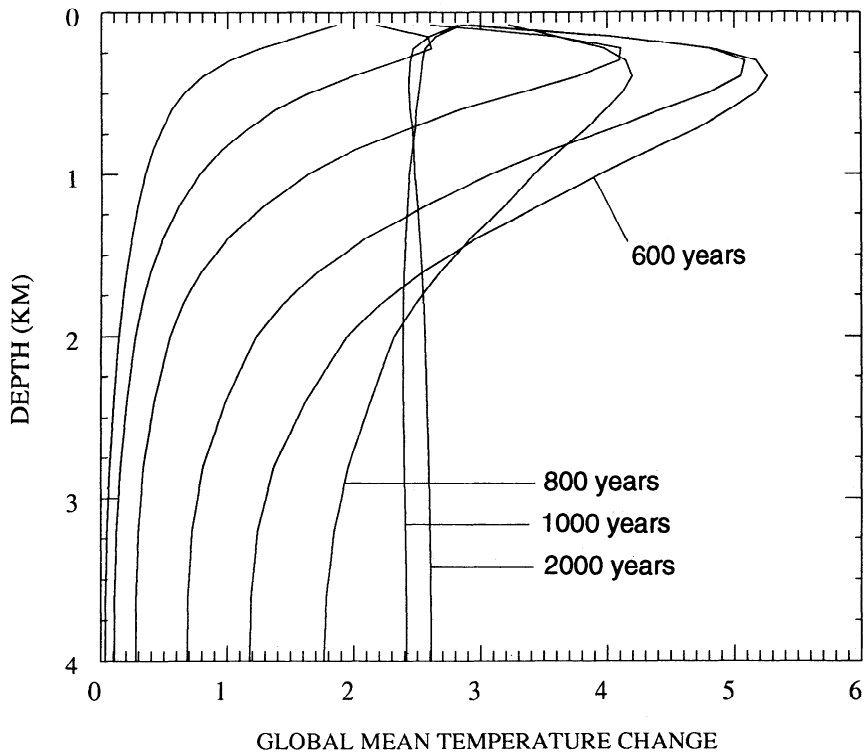

Figure 15. Globally averaged deep ocean temperature change profile at 50, 100, 200, 400, 600, 800, 1000, and 2000 years after a step function GHG increase for experiment SVU2.

unperturbed overturning. However, the salinity changes induce an overturning cell which reinforces the unperturbed circulation. Thus neither the ΔT nor ΔS field alone leads to an overall weakening of the circulation. Instead, both, acting individually, serve to intensify the local circulation but in opposite senses, and it is only their combined effect which leads to a collapsed circulation.

Finally, the circulation collapse obtained with small A_0 is similar to that obtained by *Manabe and Stouffer* [1993] for a CO_2 quadrupling using an A/O GCM with realistic land-ocean geography. The results obtained here suggest that the occurrence of a near-total circulation collapse is dependent on the value of K_v (through A_0), and is eventually followed by a sudden reinvigoration of the thermohaline overturning (Manabe and Stouffer ended their simulation after 500 years, whereas reinvigoration occurs here after 500-800 years).

Sensitivity to Rate of GHG Increase

In all of the preceding experiments a step function GHG heating perturbation was applied, and in every case a partial to near-total transient collapse of the thermohaline overturning occurred. This collapse is attributed to the greater rate of downward penetration of the thermal anomaly in downwelling than in upwelling regions, such that the meridional density gradient in the upper ocean is reduced. If the GHG heating perturbation is gradually applied one can expect a transient weakening of the thermohaline circulation to still occur if the timescale over which the heating perturbation is applied is shorter than the timescale for complete mixing of thermal anomalies (several thousand years), but the magnitude of the collapse should decrease as the rate of warming decreases. This is confirmed by Figure 16, which compares the variation in overturning intensity for experiment SVU2 for cases in which the heating perturbation increases linearly to a value of 6 W m^{-2} heating perturbation over periods of 1000, 2000, 5000, and 10,000 years. Even when the perturbation is smoothly increased over a 10,000 period there is a slight (6% at year 3000) transient weakening of the circulation. At the other extreme, implementation of the perturbation over a 200-year timescale, comparable to that associated with the anthropogenic GHG increase, simply delays the pattern of temperature change seen in Figure 14 by about 200 years, with negligible impact on the magnitude of the transient heating or cooling extremes.

The results presented here thus indicate that at geological timescales of 10^3 to 10^4 years, the impact of changes in surface climate on the deep ocean circulation during the transition from one climate to another depends on the rate of climatic change. Current anthropogenic heating perturbations, in contrast, are rapid compared to the ocean mixing timescale, so that the transient deep ocean circulation response is the same whether a step function or gradual GHG increase is applied.

Sea Level Response

Figure 17 shows the increase of sea level due to thermal expansion for the SF and SVO series of experiments. As the vertical diffusion coefficient K_v is increased in experiments SF1 to SF6 the initial surface transient response becomes progressively slower but the deep ocean response becomes faster as a result of faster heat uptake by the oceans (Figure 2). This implies that, to the extent that smaller transient warming over the coming decades is a result of greater ocean heat uptake rather than a smaller GHG heating perturbation or smaller climate sensitivity, a smaller realized warming will be associated with a faster sea level rise. By year 200, sea level rise is 4 times larger for SF6 than for SF1 while surface warming is only one quarter smaller (Figure 2a). The greater sensitivity of transient sea level rise than surface warming to K_v (and hence to rate of ocean heat uptake)

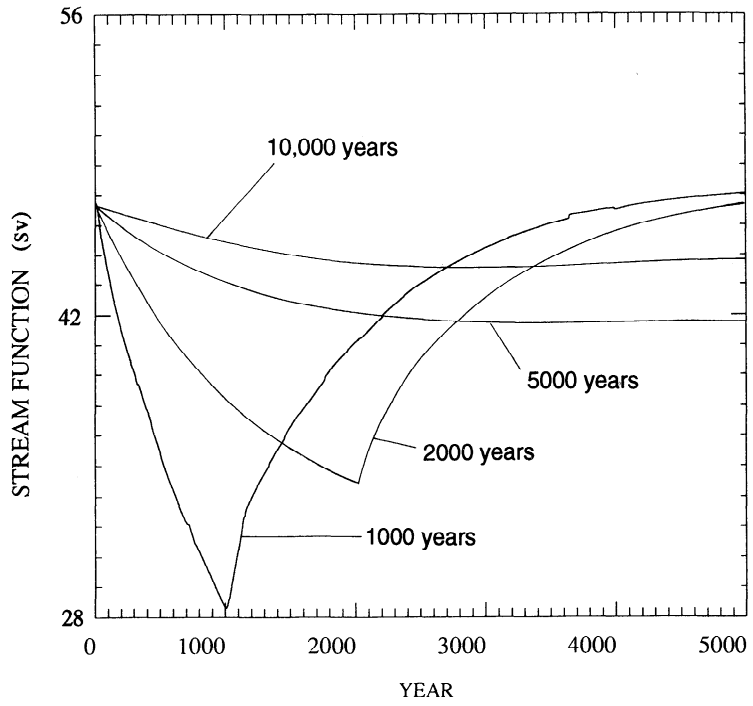

Figure 16. Variation of maximum stream function value for experiment SVU2 when a heating perturbation is linearly increased to a value of 6 W m^{-2} over periods ranging from 1000 to 10,000 years.

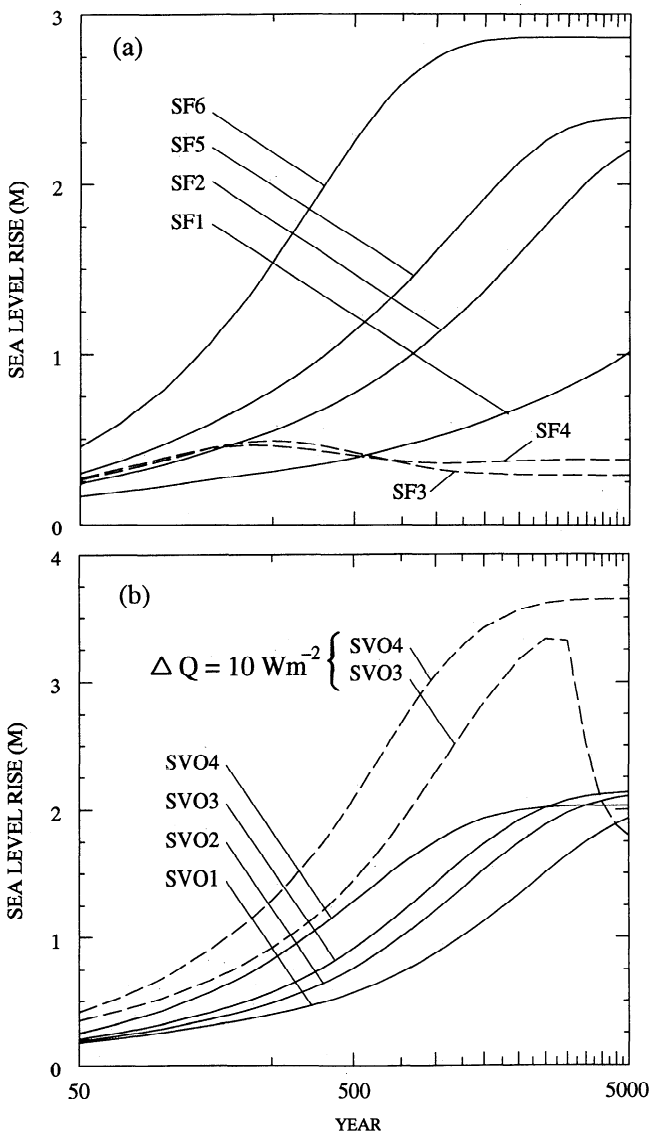

Figure 17. Sea level rise following a 6 W m^{-2} step function heating perturbation for (a) experiments SF1 to SF6 and (b) experiments SVO1 to SVO4 for a heating perturbation of 6 W m^{-2} (solid lines) or 10 W m^{-2} (dashed lines).

arises because the relative difference in transient warming between SF1 and SF6 increases with increasing depth. Thus relatively small differences in the transient surface temperature response due to differences in ocean mixing can be associated with large differences in transient sea level rise.

Experiments SF3 and SF4 (Figure 17a) and SVO3.Q10 (Figure 17b) represent departures from the correlation between surface temperature transient response and sea level rise established by the other experiments. In all three cases, a second overturning cell develops during the transient. This simultaneously accelerates the surface temperature response and suppresses deep ocean warming, so that limited sea level rise is associated with a relatively rapid surface transient response. Indeed, sea level falls during the later part of the transient response.

Table 5 gives the steady state sea level rise for experiments SF2, SF5, and SF6, as well as the times required to reach 50% and 75% of the steady state rise. If the circulation is qualitatively unchanged after a warming, an eventual sea level rise of 2 to 3 m occurs and depends only weakly on the value of K_v because the steady state temperature change profile is largely unaffected by changes in K_v. This rise is entirely due to thermal expansion and is in addition to sea level rise that might occur in reality due to melting or calving of glaciers and ice sheets. The timescale for sea level rise is substantially longer than the surface temperature response timescale, ranging from about 200 to 1100 years for 50% response, and from about 400 to 2400 years for a 75% response (and even longer for experiment SF1, which was not run to steady state).

The steady state sea level rise in experiment SF6 is greater than that in experiment SF5 (Figure 17a) in spite of the fact that the global mean ocean warming is greater in experiment SF5 (Figure 2b). However, the warming in the upper ocean is greater in experiment SF6 (Figure 3) and, because the thermal expansion coefficient is larger at warmer temperatures, this leads to a greater sea level rise than in experiment SF5 in spite of the smaller mean ocean warming. Hence the correlation between sea level rise and ocean warming is imperfect because sea level rise is most influenced by the warming in the upper ocean, and different experiments with similar mean warming can have different vertical warming profiles.

The steady state sea level rise and response timescales obtained here are, in most cases, substantially larger than obtained by *Mikolajewicz et al.* [1990] using the Hamburg geostrophic ocean general circulation model. For a mean ocean surface warming of 4°C, they obtain a steady state sea level rise of 0.51 m, with 50% and 75% responses obtained after 80 and 210 years, respectively. These differences imply that the steady state ocean temperature warming decreases with increasing depth in their model, unlike the near-uniform warming obtained here. *Manabe and Bryan* [1985], in contrast, observe that the steady state deep ocean warming after a CO_2 increase in their coupled A/O GCM is significantly larger than the mean surface warming. Since their surface climate sensitivity is comparable to that obtained here, this pattern implies an even larger sea level rise than obtained here. Until the likely variation of ocean warming with depth can be constrained, a large uncertainty will remain concerning the ultimate sea level rise due to thermal expansion associated with a given surface warming.

In summary, the key results obtained here are (1) the rate of sea level rise varies inversely with the rate of surface warming; (2) the response time constant is of the order of 10^3 - 10^4 years; (3) an eventual rise due to thermal expansion alone of 2-3 m occurs in response to a 6 W m^{-2} heating

Table 5. Steady State Sea Level Rise and Times Required to Reach 50% and 75% of the Steady State Rise for Selected Experiments

Experiment	Sea Level Rise, m	Response Times, years	
		50%	75%
SF2	2.3	1060	2380
SF5	2.4	560	1280
SF6	2.9	230	440
SF3	0.3	---	---
SF4	0.4	---	---

perturbation; (4) the sea level rise is most influenced by the warming in the upper ocean, where the thermal expansion coefficient is largest; (5) the response can vary nonlinearly with the heating perturbation; and (6) an initial sea level increase can be followed by falling sea level if a new overturning cell, which adds cold water to the deep ocean, develops.

Impact of Ice and Snow Feedback

Introduction of ice and snow causes the atmospheric temperature response to external forcing changes to be locally amplified by about a factor of 2 relative to the global mean response but suppresses the mixed layer temperature response poleward of the ice limits that exist in the new steady state. This has only a minor effect on τ_e. The deep ocean temperature change is largely governed by the temperature change in downwelling regions, which occur equatorward of the ice edge. As ice retreats the downwelling zone shifts poleward but mixed layer warming in the region which becomes ice-free is not suppressed. As a result, the profile of deep ocean temperature change, and the associated sea level rise, is unaffected by the presence of sea ice.

Discussion and Conclusions

This paper presents and analyzes the transient temperature and sea level response of a two-dimensional (latitude-depth) ocean model which is coupled to an energy balance surface-atmosphere climate model. Most of the experiments presented here involved application of a step function greenhouse gas (GHG) surface-troposphere heating perturbation of 6 W m^{-2}. Because the models used here are highly simplified, the ocean model in particular consisting of a single zonally averaged basin and forced by fixed wind stress and a fixed precipitation pattern, great confidence cannot be placed in the quantitative results obtained here. Rather, the focus of the present investigation is to gain further insight into a range of possible transient response behaviors and to compare the 2-D model with the widely used one-dimensional upwelling-diffusion and box diffusion models.

The key findings of the present study are as follows:

1. A weakening of the thermohaline circulation occurs during the first 100 years of the transient response to a step function GHG increase in all cases examined here, the weakening being a result of greater downward penetration of the warming anomaly in downwelling than in upwelling regions rather than a result of reduced convection.

2. Applying the GHG increase over a period of several hundred years delays but does not reduce the magnitude of the circulation collapse.

3. The transient weakening of the thermohaline circulation substantially slows surface warming at high latitudes in the hemisphere(s) where sinking occurs as a result of the associated reduction in meridional heat transport. The transient circulation weakening also slows the global mean surface response, as additional heat is able to diffuse into the deep ocean.

4. A temperature warming can induce a transition from a one-cell to a two-cell overturning regime if the model is close to the boundary between these regimes. In this case the development of a second overturning cell accelerates the surface transient temperature response and leads to a greater high-latitude response in the latitude where the new cell develops.

5. In some cases, involving sufficiently small (but realistic), stability-dependent K_v and latitudinally uniform ocean fraction and precipitation, the unperturbed circulation consists of a single overturning cell spanning both hemispheres and the transient circulation collapse is large enough to induce temporary cooling at high latitudes in the hemisphere where sinking occurred. During this period the largest warming (up to twice the concurrent globally averaged surface response) occurs at a depth of 400-800 m in the ocean. This is followed by a sudden reintensification of the circulation after 700-1000 years which transfers heat from the deep ocean to surface, causing the high-latitude surface temperature change in both hemispheres to overshoot its steady state response by up to 50% before relaxing to the steady state response.

6. The e-folding timescale τ_e for the global mean surface temperature response ranges from 10 years with K_v fixed at 1×10^{-5} m^2 s^{-1} to 142 years for K_v fixed at 5×10^{-4} m s^{-1}. However, τ_e decreases and then abruptly increases as K_v increases from 5×10^{-5} m^2 s^{-1} to 1×10^{-4} m^2 s^{-1} due to differences in the circulation response.

7. The transient surface response of both the 1-D upwelling-diffusion model and the pure diffusion ocean model is significantly faster than that of the 2-D model, due to the transient weakening of overturning circulation which occurs in the 2-D model. The 1-D model can be made to replicate the transient response of the 2-D if the transient circulation weakening from the 2-D model is imposed in the 1-D model.

8. The occurrence of convection has a substantially smaller effect on the transient surface temperature response than expected based on 1-D model simulations. This is attributed to the fact that the transient weakening of the overturning circulation is smaller in the presence of convection and to the fact that convection occurs where strong downwelling also occurs, so that thermal anomalies are mixed deeply for model versions with and without convection permitted.

9. The transient sea level rise due to thermal expansion is significantly more sensitive to changes in the vertical diffusion coefficient K_v than is the transient surface temperature response. As K_v increases from 1×10^{-5} m s^{-1} to 5×10^{-4} m s^{-1}, the sea level rise 200 years after applying a step function GHG increase quadruples while the surface temperature response decreases by only one quarter. Thus relatively small differences in the surface temperature transient response due to differences in ocean mixing can be associated with large differences in the transient sea level rise.

10. The steady state ocean warming obtained here is approximately uniform with depth and equal to the surface warming (3°C for a 6 W m^{-2} perturbation) for experiments in which the circulation is qualitatively unchanged. However, if a second overturning cell develops, the warming decreases sharply with increasing depth due to the additional source of relatively cold water to the deep ocean.

11. In cases where the ocean warming is roughly uniform with depth, sea level rises 2 to 3 m due to thermal expansion alone in response to a 6 W m^{-2} heating perturbation. However, the timescale for sea level rise is significantly longer than the timescale for surface temperature response, with the time required to reach 50% of the steady state rise ranging from 200 to 1100 years and the time to reach 75% of the steady state response ranging from 500 to several thousand years.

12. When ice and snow cover are permitted at high latitudes, the high-latitude atmospheric temperature response is

amplified (due primarily to thinning of sea ice) but the mixed layer temperature response in regions where bottom water forms prior to the GHG perturbation (which are ice-free) is not amplified. Hence the presence of sea ice has negligible effect on the deep ocean warming and associated sea level rise.

The near-total circulation collapse obtained here with small, stability-dependent K_v is similar to that obtained by *Manabe and Stouffer* [1993] for CO_2 quadrupling using an A/O GCM. The sensitivity experiments presented here may provide important insights into the GCM results, in that they suggest that the circulation collapse is dependent on the value of K_v and is eventually followed by a sudden reinvigoration of thermohaline overturning. *Manabe and Stouffer* [1993] extended their integration for 500 years, whereas reinvigoration of the circulation occurs here after 500-800 years.

The climate-circulation feedback obtained here is not consistent with that hypothesized by *Gaffin et al.* [1986] and utilized by *Piehler and Bach* [1992]. They assume that the upwelling velocity initially increases as climate warms, whereas here, the upwelling velocity decreases with warming as the overall circulation intensity weakens. However, the initial upwelling increase postulated by *Gaffin et al.* [1986] is assumed to represent the effect of a strengthened Hadley circulation and associated Ekman-induced upwelling, a feedback which is omitted from the present model. Whether this hypothesized feedback can temporarily over-ride the substantial weakening of the thermohaline overturning obtained here and result in a net deep-ocean-to-surface heat flux during the early transient requires study with a fully interactive atmosphere-ocean model. A two-dimensional statistical-dynamical atmospheric model with an interactive hydrological cycle and internally predicted, zonally averaged winds is currently under development (L. D. D. Harvey, A two-dimensional zonally averaged atmosphere-land surface model for longterm climate simulations, manuscript in preparation) and will be applied to this question in a future study.

The results obtained here might have implications for the dynamics of warming during glacial-interglacial oscillations and for the Younger Dryas oscillation which occurred at the end of the last ice age. A partial to near total transient collapse of the thermohaline overturning is a persistent feature of warming which occurs faster than the ocean mixing timescale, and could therefore occur in reality even without a meltwater pulse (which has been widely invoked to explain a North Atlantic circulation collapse inferred to have occurred during the Younger Dryas, as discussed by *Harvey* [1989] or poleward shift of the baroclinic precipitation belt. Such collapse can induce middle to high-latitude cooling of several centuries duration, which is comparable to the timescale of the Younger Dryas, while the rest of the planet and deep ocean continue to warm. If circulation collapses are driven by warming itself rather than by changes in freshwater inputs, this could explain the absence of a circulation collapse during the post-Younger Dryas meltwater pulse into the North Atlantic [see Teller, 1990].

A number of studies suggest that much of the bottom water in the world ocean originates as surface water whose density is increased through a combination of surface cooling, net evaporation, and brine ejection in regions of net sea ice formation [Smith, 1975; Killworth, 1977; Foster et al, 1987]. These dense waters sink down continental slopes as boundary layer plumes, a process not included in global ocean GCMs nor in the present model. Because polar boundary layer plumes provide a mechanism by which surface waters in regions of sea ice cover can be transmitted to the deep ocean, and because the temperature of this source water is closely tied to the freezing point of sea water, their incorporation in global models might result in a deep ocean warming which is substantially smaller than the global mean mixed layer warming as long as sea ice still occurs in the source regions for the plumes. This possibility was discussed by *Harvey and Schneider* [1985] and will be investigated in a future study in which a simple polar plume model will be added to the present model.

Acknowledgments. This research was supported by Natural Sciences and Engineering Research Council (Canada) grant OPG0001413.

References

Bretherton, F.P., K. Bryan, and J.D.Woods, Time-dependent greenhouse-gas-induced climate change, in *Climate Change: The IPCC Scientific Assessment*, edited by J.T. Houghton, G.J. Jenkins, and J.J. Ephraums, pp. 173-193, Cambridge University Press, New York, 1990.

Bryan, F., Parameter sensitivity of primitive equation ocean general circulation models, *J. Phys. Oceanogr., 17*, 970-985, 1987.

Foster, T.D., A. Foldvik, and J.H. Middleton, Mixing and bottom water formation in the shelf break region of the southern Weddell Sea, *Deep Sea Res., 34*, 1771-1794, 1987.

Friedrich, H., and S. Levitus, An approximation to the equation of state for sea water, suitable for numerical ocean models, *J. Phys. Oceanogr., 2*, 514-517, 1972.

Gaffin, S.R., M.I. Hoffert, and T. Volk, Nonlinear coupling between surface temperature and ocean upwelling as an agent in historical climate variations, *J. Geophys. Res., 91*, 3944-3950, 1986.

Gargett, A.E., Vertical eddy diffusivity in the ocean interior, *J. Mar. Res., 42*, 359-393, 1984.

Harvey, L.D.D., Effect of ocean mixing on the transient climate response to a CO_2 increase: Analysis of recent model results, *J. Geophys. Res., 91*, 2709-2718, 1986.

Harvey, L.D.D., A semi-analytic energy balance climate model with explicit seaice and snow physics, *J. Clim., 1*, 1065-1085, 1988a.

Harvey, L.D.D., Development of a sea ice model for use in zonally averaged energy balance climate models, *J. Clim., 1*, 1221-1238, 1988b.

Harvey, L.D.D., Modelling the Younger Dryas, *Quat. Sci. Rev., 8*, 137-149, 1989.

Harvey, L.D.D., A two dimensional ocean model for long-term climatic simulations: Stability and coupling to atmosphere and sea ice models, *J. Geophys. Res., 97*, 9435-9453, 1992.

Harvey, L.D.D., and S.H. Schneider, Transient climatic response to external forcing on 10^0- 10^4 year time scales, 1, Experiments with globally averaged coupled atmosphere and ocean energy balance models, *J. Geophys. Res., 90*, 2191-2205, 1985.

Henderson-Sellers, B., Modelling sea surface temperature rise resulting from increasing atmospheric carbon dioxide concentrations, *Clim. Change, 11*, 349-359, 1987.

Kiehl, J.T., and V. Ramanathan, Radiative heating due to

increased CO_2: The role of H_2O continuum absorption in the 12-18 μm region, *J. Atmos. Sci., 39*, 2923-2926, 1982.

Killworth, P.D., Mixing on the Weddell Sea continental slope, *Deep Sea Res., 24*, 427-448, 1977.

Manabe, S., and K. Bryan, CO_2-induced change in a coupled ocean-atmosphere model and its paleoclimatic implications, *J. Geophys. Res., 90*, 11689-11707, 1985.

Manabe, S., and R.J. Stouffer, Century-scale effects of increased atmospheric CO_2 on the ocean-atmosphere system, *Nature, 364*, 215-218, 1993.

Manabe, S., R.J. Stouffer, M.J. Spelman, and K. Bryan, Transient responses of a coupled ocean-atmosphere model to gradual changes of atmospheric CO_2: Part I: Annual mean response, *J. Clim., 4*, 785-818, 1991.

Manabe, S., M.J. Spelman, and R.J. Stouffer, Transient responses of a coupled ocean-atmosphere model to gradual changes of atmospheric CO_2, II, Seasonal response, *J. Clim., 5*, 105-126, 1992.

Mikolajewicz, U., B.D. Santer, and E. Maier-Reimer, Ocean response to greenhouse warming, *Nature, 345*, 589-593, 1990.

Piehler, H., and W. Bach, The potential role of an active deep ocean for climatic change, *J. Geophys. Res., 97*, 15507-15512, 1992.

Schlesinger, M.E., and X. Jiang, The transport of CO_2-induced warming into the ocean: An analysis of simulations by the OSU coupled atmosphere-ocean general circulation model, *Clim. Dyn., 3*, 1-17, 1988.

Semtner, A.J., A model for the thermodynamic growth of sea ice in numerical investigations of climate, *J. Phys. Oceanogr., 6*, 379-389, 1976.

Smith, P.C., A streamtube model for bottom boundary currents in the ocean, *Deep Sea Res., 22*, 853-873, 1975.

Stouffer, R.J., S. Manabe and K. Bryan, Interhemispheric asymmetry in climate response to a gradual increase of atmospheric CO_2, *Nature, 342*, 660-662, 1989.

Teller, J.T., Volume and routing of late-glacial runoff from the southern Laurentide ice sheet, *Quat. Res. N.Y., 34*, 12-23, 1990.

Washington, W.M., and G.A. Meehl, Climate sensitivity due to increased CO_2: experiments with a coupled atmosphere and ocean general circulation model, *Clim. Dyn., 4*, 1-38, 1989.

Watts, R.G., Global climate variation due to fluctuations in the rate of deep water formation, *J. Geophys. Res., 90*, 8067-8070, 1985.

Watts, R.G., K. Morantine, and K. Achutarao, Time scales in energy balance climate models, 1, The limiting case solutions, *J. Geophys. Res., 99*, 3631-3641, 1994.

Wigley, T.M.L. and S.C.B. Raper, Natural variability of the climate system and detection of the greenhouse effect, *Nature, 344*, 324-327, 1990.

Wright, D.G., and T.F. Stocker, A zonally averaged ocean model for the thermohaline circulation, I, Model development and flow dynamics, *J. Phys. Oceanogr., 21*, 1713-1724, 1991.

L.D.D. Harvey, Department of Geography, University of Toronto, 100 St. George St., Toronto, Ontario, Canada M5S 1A1. (e-mail: harvey@harvey.geog.utoronto.ca)

(Received July 19, 1993; revised November 14, 1993; accepted December 7, 1993.)